Motion Compensated Continuous Blood Pressure Measurements Using Recurrent Neural Networks

by

Shrimanti Ghosh

A thesis submitted in partial fulfillment of the requirements for the degree of

Master of Science

Department of Computing Science

University of Alberta

Abstract

High blood pressure (BP) is the leading cause of death and disability in the world, affecting nearly 1.5 billion adults. It leads to many complications, including stroke, heart failure, kidney disease, and coronary disease. In current clinical practice, BP is measured either invasively by an intra-arterial catheter that is invasive and causes pain or non-invasively by cuff using the oscillometric method, which does not allow continuous BP measurement. Therefore, development of an accurate, continuous, and non-invasive BP measurement method is needed for hypertension diagnosis and management.

Prediction models based on pulse transit time (PTT) have been used for continuous and non-invasive BP estimation. PTT has been reported to be highly correlated with BP, which makes PTT a good candidate to be used for continuous BP monitoring, including for continuous ambulatory monitoring. PTT can be defined as the time lag between the R-peak of the ECG signal and the peak of the blood oxygenation signal (PPG) signal, when measured within the same cardiac cycle. In this study, windowed cross-correlation between the adjacent peak points of ECG and PPG signals in the same cardiac cycle is used to compute PTT automatically. We have performed sparsification of PPG signal by computing a moving window maximum on that signal. This pre-processing converts the PPG signal into a very sparse signal that ultimately increased the accuracy and the efficiency of PTT calculation. We then use a linear regression model to calculate BP continuously from PTT measurement where unknown constants of that model are subject dependent and must be calibrated.

To improve the classical PTT-based prediction during motion, along with the ECG and the PPG signals, for the first time to our knowledge, we use

signals from accelerometers and gyroscopes to predict BP. Accelerometers and gyroscopes have been widely accepted as useful and practical sensors for wearable devices to measure and assess physical activity. To make a prediction model, we use recurrent neural networks (RNNs), which can effectively learn the multi-timescale dependencies from a sequential time series of BP values. For this study, deep long short-term memory network (LSTM) and gated recurrent units (GRU) were used.

BP was monitored in five different scenarios (seating, standing, recumbent, walking and cycling) from 50 healthy volunteers. We propose that the RNN models can predict continuous BP sequences from physiological signals like ECG, PPG and other parameters like PTT in posture and activity. Walking and cycling introduce baseline noise into both the ECG and PPG signals, making it more difficult to accurately estimate the BP values. To predict BP more accurately during activity, here we incorporated the accelerometric and gyroscopic values in the model. After including these data, we are able to achieve significant boost in the accuracy for all positions. The mean $\pm$ standard deviation is 0.08 $\pm$ 4.5 for SBP and 1.7 $\pm$ 3.4 for DBP in seated position and 2.3 $\pm$ 5.7 for SBP and 2.5 $\pm$ 4.2 for DBP while walking which is permissible according to the accepted threshold for accuracy using GRUs. Also, the root mean squared error between the reference standard and estimated SBP and DBP are 4.22 and 3.73 respectively for motionless position and are 6.10 and 4.80 for walking in case of GRUs. It can be stated that the difference between the estimated BP from RNN and the reference standard was less than the accepted threshold in all scenarios. The deep learning based method applied in this study appears sufficiently accurate in measuring BP not only in motionless conditions but also for walking and cycling, where motion artefacts are present. This novel approach has a significant potential contribution in continuous BP measurement in different postures and activity for hypertension management.

Preface

This is a collaborative project between the Department of Computing Science and the Department of Medicine of the University of Alberta.

The research project, of which this thesis is a part, received research ethics approval from the University of Alberta Research Ethics Board, Project Name, 'Pulse Transit Time as a Predictor of Blood Pressure', Pro00063510, 29 April 2016.

The results of the thesis were published at 2018 IEEE International Conference on Acoustics, Speech and Signal Processing, IEEE-NIH 2016 Special Topics Conference on Healthcare Innovations and Point-of-Care Technologies and at Canadian Hypertension Congress in 2016 and 2017.

I myself have reported all the major work as the primary author here and was responsible for implementation, experimentation and analysis.

To my family, especially my mom

For your infinite love and support at each step of my life ...

Acknowledgements

Regarding my thesis directors, I am specially indebted to my respected supervisors Professor Pierre Boulanger and Professor Raj Padwal for their sincere supervision and valuable guidance which helped me to complete this project.

I am also grateful to Peter Wood to teach me the clinical aspect of this project and for his constant support during the rigorous data collection process.

I am thankful to Ankur Banerjee for his proper assistance in collecting the clinical data from a large number of people.

I would like to express my gratitude specially to Professor Nilanjan Ray for his kind support and encouraging motivation regarding the application of deep learning techniques in our project.

This is last but not the least thanksgiving to all of my colleagues, lab mates and friends for their honest cooperation whenever I needed.

Table of Contents

1 Introduction **1**
- 1.1 Motivation . . . 3
- 1.2 State-of-the-Art in BP Measurements . . . 5
- 1.3 Thesis Objectives . . . 6
- 1.4 Thesis Contributions . . . 7
  - 1.4.1 Contribution . . . 7
  - 1.4.2 Papers accepted and published at conferences . . . 7

2 Related Work **9**
- 2.1 Other BP Measurement Methods . . . 11

3 Measuring Real-time Physiological Signals **13**
- 3.1 BioRadio Configuration . . . 13
- 3.2 BioCapture Software . . . 14
- 3.3 Measurement of Motion Data . . . 15

4 Calculation of Pulse Transit Time (PTT) **16**
- 4.1 What is Pulse Transit Time (PTT)? . . . 16
  - 4.1.1 Electrocardiogram (ECG) Signal . . . 16
  - 4.1.2 Photoplethysmogram (PPG) Signal . . . 17
- 4.2 Automated PTT Calculation . . . 19
  - 4.2.1 Processing ECG and PPG signals . . . 19
  - 4.2.2 Windowed Cross-correlation to Compute PTT . . . 22
- 4.3 Evaluation of the Accuracy of the PTT Algorithm . . . 26

5 From Pulse Transit Time to Blood Pressure Measurements **30**
- 5.1 Incorporating Accelerometric and Gyroscopic Values along with PTT . . . 32
- 5.2 Calibration Protocol . . . 32
- 5.3 Calibration Algorithm . . . 33
- 5.4 Measurements of Pilot Study Data . . . 33
  - 5.4.1 Initial Pilot Study . . . 33
  - 5.4.2 Large-Scale Study . . . 34
- 5.5 Estimation of Blood Pressure Using PTT Calibration Linear Model . . . 35
  - 5.5.1 The initial pilot study with 14 subjects . . . 35
  - 5.5.2 Large-scale study with 50 volunteers . . . 37

6 Estimation of Blood Pressure from Recurrent Neural Networks - LSTM case **40**
- 6.1 Recurrent Neural Network Model . . . 41
- 6.2 LSTM Network Training Algorithm . . . 44

7 Estimation of Blood Pressure from Recurrent Neural Networks - GRU case **48**
7.1 Gated Recurrent Unit Model 49
7.2 Difference Between LSTM vs GRU 50
7.2.1 Discussion 51
7.3 GRU Network Algorithm 52

8 Conclusion **55**
8.1 Discussion 55
8.2 Future Work 57

Bibliography **58**

List of Tables

4.1 Comparing the automated PTT and the manual PTT Mean ± SD of relative % error 28

5.1 RMSE Comparison in mmHg between measured and calculated SBP with and without sparsity. 35
5.2 RMSE Comparison in mmHg between measured and calculated DBP with and without sparsity 36
5.3 Performance results of different positions on all subjects (Mean value ± Standard deviation) 36
5.4 Comparison of RMSE values between the reference standard and estimated SBP with and without accelerometric and gyroscopic data 38
5.5 Comparison of RMSE values between the reference standard and estimated DBP with and without accelerometric and gyroscopic data 38
5.6 Comparison of Mean ± SD between the reference standard and estimated SBP with and without accelerometric and gyroscopic data 39
5.7 Comparison of Mean ± SD between the reference standard and estimated DBP with and without accelerometric and gyroscopic data 39

6.1 Comparison of RMSE values between the reference standard and estimated SBP with and without accelerometric and gyroscopic data 45
6.2 Comparison of RMSE values between the reference standard and estimated DBP with and without accelerometric and gyroscopic data 45
6.3 Comparison of Mean ± SD between the reference standard and estimated SBP with and without accelerometric and gyroscopic data 46
6.4 Comparison of Mean ± SD between the reference standard and estimated DBP with and without accelerometric and gyroscopic data 46

7.1 Comparison of RMSE values between the reference standard and estimated SBP with and without accelerometric and gyroscopic data 54
7.2 Comparison of RMSE values between the reference standard and estimated DBP with and without accelerometric and gyroscopic data 54
7.3 Comparison of Mean ± SD between the reference standard and estimated SBP with and without accelerometric and gyroscopic data 54

7.4 Comparison of Mean ± SD between the reference standard and estimated DBP with and without accelerometric and gyroscopic data 54

List of Figures

3.1 BioRadio Primary Module and Sensor Pod 14
3.2 Various physiological signal acquisition from the BioCapture Software 15

4.1 Definition of Pulse Transit Time 17
4.2 Electrocardiogram signal 18
4.3 Photoplethysmogram signal 18
4.4 An example of clean synchronized ECG (in blue) and PPG (in red) signals 19
4.5 Another example of clean synchronized ECG (in blue) and PPG (in red) signals 20
4.6 Example of a noisy ECG and PPG signal captured during walking 21
4.7 Example of a noisy ECG and PPG signal captured during cycling 22
4.8 ECG(blue) and PPG(red) signals 25
4.9 PPG signal with maxima(red) and ECG signal 26
4.10 Graph of correlation coefficients in one window 27
4.11 ECG signal (setting the threshold manually) 28
4.12 PPG signal (setting the threshold manually) 29
4.13 Automated PTT(red) with Manual PTT(blue) 29

5.1 Bland-Altman plot of SBP of all 14 subjects obtained during seated (*), standing (o), walking (+). 37
5.2 Bland-Altman plot of DBP of all 14 subjects obtained during seated (*), standing (o), walking (+). 37

6.1 LSTM many-to-one architecture 43
6.2 LSTM many-to-many architecture 43
6.3 LSTM model summary and the parameters 45
6.4 Loss - MSE vs. Epoch curve for training and validation for the LSTM 46

7.1 Visual representation of (a) LSTM and (b) GRU 51
7.2 Loss - MSE vs. Epoch curve for training and validation for the GRU 53

Whatever the mind of man can conceive and believe, it can achieve.

– Oliver Napoleon Hill, American author.

Chapter 1

Introduction

High blood pressure (BP) is the most common cause of death or disability world-wide and a major risk factor for a number of serious diseases, including cardiovascular and kidney disease [1]. High BP detection and control rates are extremely low, especially in low resource settings [2]. In current clinical practice, BP measurement is performed either invasively by an intra-arterial catheter or non-invasively by cuff using either oscillometric or auscultatory methods. Invasive measurement is continuous in nature but carries risk (infection, bleeding, thrombosis) and is used only for critically ill patients and not for patients with chronic hypertension. Intermittent cuff inflation, the gold standard for BP measurement in chronic hypertension, is non-invasive but does not allow for continuous blood pressure measurement [3]. *Development of an accurate continuous non-invasive BP measurement technique would revolutionize hypertension diagnosis and disease management [4].*

Recently, various machine learning algorithms have been employed to improve medical diagnosis, including predicting the risk of stroke and coronary heart diseases [5, 6]. Further, there are mounting evidences that pulse transit time (PTT i.e., the time delay for the pressure wave to travel between two arterial sites) can provide the basis for convenient cuff-less BP measurement [3]. Although major progress has been made on PTT-based BP monitoring techniques, further research is still required to solve many issues associated with this measurement technique.

PTT is the time that takes the pulse pressure waveform to propagate

through a length of the arterial tree [7]. PTT can be defined as the time between the R-peak of the electrocardiogram (ECG) signal and the peak of the photoplethysmogram (PPG) signal, when measured within the same cardiac cycle [4]. The PTT-based approach for cuff-less BP monitoring has captured the interest of many investigators. Many studies employed waveform measurement methods for cuff less and automated BP monitoring in general [8]. The classical PTT estimation methods employ feature detection and have been applied for cuff less BP monitoring [8].

In this study, a customized algorithm was designed to compute PTT automatically. Cross-correlation between the adjacent peak points of ECG and PPG signals in the same cardiac cycle was used to compute PTT [9]. Accuracy and the efficiency were increased when sparsified, preprocessed PPG signals were used. Then BP was measured using linear BP-PTT relationship. This BP estimation was reasonably accurate while stationary but not during motion (with RMSE of 5.7 mmHg in stationary and 7.47 mmHg during motion).

To improve the accuracy of the linear model for BP prediction during motion we use signals from accelerometers and gyroscopes along with ECG and PPG signals to compute PTT. Accelerometers and gyroscopes have been widely accepted as useful and practical sensors for wearable devices to measure and assess physical activity [10]. To make a better prediction model, we used recurrent neural networks (RNNs), which can effectively learn the multi-timescale dependencies from a sequential time series of BP values. Deep long short-term memory network (LSTM) and gated recurrent unit (GRU) were employed here. The RMSE achieved from GRUs are 4.22 and 6.10 for stationary and during motion respectively. RNNs are the family of neural networks useful for processing temporal sequential data and have been successfully used in various sequence learning tasks to model long-term dependencies. The neural network is able to discover the latent correlation between different time series and learn from the dependency and predict the target values. This problem can be framed as a multivariate temporal sequence prediction problem and an appropriate application of biomedical signal processing. We used sequence-to-sequence learning framework to solve this problem [11].

1.1 Motivation

Blood pressure acts as one of the vital signs providing the useful information about cardiac output and elasticity of the blood vessel and physiological variation. Therefore, the measurement of BP is helpful for a physician to understand and diagnose the integrity function of the cardiovascular system. The invasive method of measuring the blood pressure by inserting a catheter into the blood vessel to measure the arterial pressures accurately, still has the disadvantage of accompanying pain and contamination, and the side effects arising from inserting the catheter-tip into a patient's blood vessel. The various indirect methods of measuring BP such as Riva-Rocci, oscillometric, ultrasound, tonometry method, etc. were developed as possible solutions these problems [12, 13].

However, there is the inconvenience of using the cuff attached to the patient's arm for non-invasive BP measurement and also the limitation in measuring the blood pressure continuously. Recently, the continuous and non-invasive BP measurements using PTT, in inversely linear relationship with blood pressure, have been extensively explored in the past few decades. Methods for continuously monitoring blood pressure from other physiological parameters have been widely studied. Most of these studies correlate blood pressure (BP) with PTT [14]. For continuous measurement of blood pressure by this method, constant patient dependent calibration coefficients are needed in addition to the continuous extraction of PTT [15].

Current blood pressure devices (by oscillometry or sphygmomanometery) are mainly based on air-cuff, which only can measure blood pressure intermittently and may not be suitable for long term blood pressure monitoring. Therefore, cuff less blood pressure monitoring method would be valuable in stroke prevention and management. As an important risk factor, blood pressure has prognostic value for stroke [3]. Continuous blood pressure measurement can be used to assist for the preventing and predicting of stroke [3]. In particular, cuffs are cumbersome and time consuming to use, disruptive during ambulatory monitoring, especially while sleeping, and do not readily extend

to low resources settings.

Research is surely needed to improve the calibration of PTT to BP in terms of accuracy and convenience. Methods involving a BP perturbing intervention or frequent re-calibration with a cuff may be hard to adopt. One potential method is universal calibration, wherein the parameters of the model relating PTT to BP are determined simply from the subject's age, gender, and other such information including cardiovascular risk factors. To enhance the accuracy without significantly compromising convenience, a single cuff BP measurement could be obtained from the subject every so often. Also research is needed to enable independent determination of systolic and diastolic BP. A single PTT measure cannot indicate these two BP values when they are not varying in the same direction (e.g., isolated systolic hypertension) [8].

Most experiments were based on signal processing on collections of data [16]. Only a few authors investigated new solutions and devices for blood pressure measurement based on PTT [16].

Existing methods for cuffless and continuous BP estimation are pulse transit time model [17, 18], and regression model, such as decision tree, support vector regression and etc [19, 20]. These models suffers from accuracy decay over time, especially for multi-day continuous BP prediction. Such limitation has become the bottleneck that prevents the use of these models in practical applications. It is worth to mention that the aforementioned models directly map present input to the target while ignoring the important temporal dependencies in BP dynamics. This could be the root of long-term inaccuracy.

While much progress has been made on ubiquitous BP monitoring via PTT, significant work is still needed to best realize this approach in practice. Also, from Computing Science perspective, latest deep learning methods based on deep neural networks have not been significantly applied to predict BP continuously from various physiological signals. For this reason we have come up with a novel approach to try to solve this problem.

In this study, we measured BP under five different conditions (recumbent, seated, standing, walking, cycling). Walking and cycling introduce baseline noise into both the ECG and PPG signals due to the presence of motion arte-

facts and have varying physiological states from resting, making it more difficult to accurately estimate the corresponding BP values. To our knowledge, no prior research study has been performed to predict BP accurately during motion. BP prediction problem can be framed as a multivariate temporal sequence prediction problem and an appropriate application of biomedical signal processing.

1.2 State-of-the-Art in BP Measurements

When we consider non-invasive and continuous measurement methods, we mean methods not needing skin penetration and the possibility to measure BP values on long time periods. For medical doctors it is necessary to find some method, which will measure accurately several parameters of systolic, diastolic, mean BP.

Noninvasive and continuous BP monitoring is not yet practically available for everyday life. It is very challenging to make the devices easily wearable as well as to reduce noise level and improve accuracy. Such devices should not only provide accurate and reliable bloop pressure measurements but also be easy to use in a convenient way that does not excessively burden the user for daily use. Variations in individual's physical characteristics and different postures increase the complexity of continuous BP monitoring, especially outside the health centre or clinic. In [21] the wrist watch based system (called BioWatch) was developed that can measure PTT and hence BP.

In [22], a PTT estimation method based on photoplethysmographic imaging (PPGi) was presented. The method utilized two opposing cameras for simultaneous acquisition of PPG waveform signals and is especially suitable for implementation in dual-camera-smartphones, which could facilitate PTT measurement among populations affected by cardiac complications.

Body sensor networks (BSNs) are widely used in medical health monitoring [23]. A smart phone centric body sensor network can help measure pulse transit time and continuously monitor blood pressure [23]. Their proposed BSN system estimates BP based on PTT, which is calculated from ECG and

PPG signals.

A cuff-less continuous BP monitoring device, which is consisted of two acquisition modules and an Android smart-phone, was presented in [24]. The data were transmitted by a Bluetooth module in the system.

Recent technological advances, such as wearable sensing and smart phones, have increased the feasibility of developing a non-intrusive continuous BP monitor system.

1.3 Thesis Objectives

Unfortunately none of these methods are reliable, accurate and comfortable for patient for continuous BP monitoring. The purpose of this study is to develop a PTT-based blood pressure estimation method with personalized model and easy implementation.

The objectives of the present study are,

- to evaluate the feasibility of PTT measurement during routine maximal cardiopulmonary exercise testing by means of standard medical equipment and
- to analyze the relation between blood pressure and PTT using both a linear and a non-linear approach.

Continuous blood pressure was estimated using a previously published linear regression model in static condition as well as during motion. Results shown that PTT-based BP estimation was reasonably accurate while stationary but not during motion.

For further improvements in estimation, deep learning based non-linear models specifically recurrent neural networks (RNNs) were implemented to predict continuous BP sequences from physiological signals like ECG, PPG and other parameters like PTT in posture and activity.

1.4 Thesis Contributions

1.4.1 Contribution

- In this study, cuff-less, continuous BP was estimated using pulse transit time during variations in posture and activity;
- The linear regression model predicted the BP from PTT comparatively better during recumbent, seated and standing positions. However, walking and cycling introduce baseline noise into the signals, which limits accurate determination of BP;
- Overall, PTT-based measurement shows promise in the seated or standing position but is inaccurate with movement;
- For further improvement, we propose that the RNN models (LSTM and GRU) can predict continuous BP sequences from physiological signals like ECG, PPG, PTT and accelerometric and gyroscopic values in posture and activity;
- The deep learning based method applied in this study appears sufficiently accurate in measuring BP not only in motionless conditions but also for walking and cycling, where motion artefacts are present. This novel approach has a significant potential contribution in continuous BP measurement in different postures and activity for hypertension management.

1.4.2 Papers accepted and published at conferences

1. Shrimanti Ghosh, Ankur Banerjee, Nilanjan Ray, Peter W Wood, Pierre Boulanger, Raj Padwal, *Using Accelerometric and Gyroscopic Data to Improve Blood Pressure Prediction from Pulse Transit Time Using Recurrent Neural Network*, 2018 IEEE International Conference on Acoustics, Speech and Signal Processing; April 2018; Calgary, Canada.
2. Shrimanti Ghosh, Ankur Banerjee, Nilanjan Ray, Peter W Wood, Pierre Boulanger, Raj Padwal, *Accuracy Analysis of Blood Pressure Prediction*

from ECG and PPG signals Using Pulse Transit Time, 2017 Canadian Hypertension Congress-Hypertension Canada; October 2017; Toronto, Ontario.

3. Shrimanti Ghosh, Ankur Banerjee, Nilanjan Ray, Peter W Wood, Pierre Boulanger, Raj Padwal, *Continuous Blood Pressure Prediction from Pulse Transit Time Using ECG and PPG Signals*, IEEE-NIH 2016 Special Topics Conference on Healthcare Innovations and Point-of-Care Technologies; November 2016; Cancun, Mexico.

4. Shrimanti Ghosh, Ankur Banerjee, Nilanjan Ray, Peter W Wood, Pierre Boulanger, Raj Padwal, *Non-Invasive and Continuous Blood Pressure Prediction from Pulse Transit Time Using ECG and PPG Signals*, 2016 Canadian Hypertension Congress-Hypertension Canada; October 2016; Montreal, Quebec.

5. Shrimanti Ghosh, Nilanjan Ray, Peter W Wood, Pierre Boulanger, Raj Padwal, *Pulse Transit Time Computation Using Signal Sparsity for Continuous Blood Pressure Prediction*, 38th Annual International Conference of the IEEE Engineering in Medicine and Biology Society; August 2016; Orlando, Florida.

Chapter 2

Related Work

Researchers have proved the validity of using a non-invasive method to measure blood pressure (BP) in various studies. Current non-invasive methods can be classified into two categories: intermittent and continuous measurement.

Intermittent measurement based on the cuff method uses two traditional techniques: auscultation and oscillometry. Continuous BP measurement methods include the volume-clamp [25, 26], tonometry-based [27, 28], and pulse transit time (PTT)-based methods.

Pulse transit time (PTT) has been reported to be correlated with blood pressure, especially for the SBP [29, 30], and has been proposed as a potential surrogate of blood pressure [18]. PTT can be measured between the characteristic points of the electrocardiography (ECG) and photoplethysmography (PPG) at peripheral sites [18]. Since ECG and PPG measurements can be implemented by wearable devices, PTT provides a very practical solution for continuous blood pressure monitoring. Numerous studies have focused on the blood pressure estimation by using PTT [31, 32] and different applications have been proposed based on the blood pressure estimation methods [33].

Experimental studies have indeed shown that 1/PTT, rather than PTT, is linearly related to BP over a wide BP range [34, 35]. But the linear model cannot provide accurate estimation because PTT was found highly correlated with SBP rather than diastolic blood pressure (DBP) [36]. An accurate model describing the relationship between PTT and blood pressure is crucial for the PTT-based blood pressure estimation. Sophisticated models were further pro-

posed to enhance the accuracy of PTT-based blood pressure estimation. Some studies investigated the relationship between PTT and blood pressure under static and exercise status [37]. Considering the relationship between PTT and blood pressure could vary from person to person, calibration was proposed by some researchers to design personalized estimation model [38]. Nevertheless, the major challenge for PTT-based blood pressure measurement is to derive a personalized estimation model. Apart from the estimation accuracy, implementation of the estimation model in a device for clinical or healthcare use is the ultimate goal. The linear mapping between PTT and blood pressure has not been proved to provide the best blood pressure estimation. However, it is still the best applicable method for approximate blood pressure trend indications.

One possible way to access blood pressure without using a cuff is to measure the velocity of propagation of pulse waves along the arterial tree. Actually, the velocity of pulse pressure waves propagating along the arterial tree depends on the value of blood pressure. Indirect measurement of blood pressure was performed by continuously measuring pulse wave velocity (PWV) [17]. The best site for measuring this velocity is located in the aorta because relationship between PWV and blood pressure is only exploitable in central elastic arteries. But it is difficult to perform non-invasively.

Along with the linear relationships, a number of studies obtained a non-linear relationship between PTT and blood pressure [39]. In [40] artificial neural network (ANN) model was developed to predict the blood pressure based on PTT. When the PTT was input to the ANN, the corresponding blood pressure value could be calculated. Recently, a research group proposed a novel deep recurrent neural network (RNN) consisting of multilayered Long Short-Term Memory (LSTM) networks, which are incorporated with a bidirectional structure to access larger-scale context information of input sequence, and residual connections to allow gradients in deep RNN to propagate more effectively [11].

Although application of deep learning or deep neural networks in predicting BP have been not successful until now.

2.1 Other BP Measurement Methods

Several BP measurement methods are now available. The main methods include catheterization, auscultation, oscillometry, volume clamping, and tonometry. Catheterization is the gold standard method [41]. This method measures instantaneous BP by placing a strain gauge in fluid contact with blood at any arterial site (e.g., radial artery, aorta). However, the method is invasive.

Auscultation is the standard clinical method [42]. This method measures systolic and diastolic BP by occluding an artery with a cuff and detecting the sounds using a stethoscope and manometer during cuff deflation. The first sound indicates the initiation of turbulent flow and thus systolic BP, while the fifth sound is silent and indicates the renewal of laminar flow and thus diastolic BP.

Oscillometry is the most popular noninvasive, automatic method for BP measurement [43, 44]. This method measures mean, diastolic, and systolic BP by also using a cuff but with a pressure sensor inside it. The measured cuff pressure not only rises and falls with cuff inflation and deflation but also shows tiny oscillations indicating the pulsatile blood volume in the artery. The amplitude of these oscillations varies with the applied cuff pressure, as the arterial elasticity is nonlinear. The BP values are estimated from the varying oscillation amplitudes by using the empirical fixedratios principle.

Volume clamping is a noninvasive, automatic method used in research [25, 26]. This method measures instantaneous (finger) BP by using a cuff and a photoplethysmography (PPG) sensor to measure the blood volume. The blood volume at zero transmural pressure is estimated via oscillometry. Measurement at the finger allows uninterrupted recordings of long duration. The transmission of the pressure pulse along the arm arteries, however, causes distortion of the pulse waveform and depression of the mean blood pressure level. Finger arteries are affected by contraction and dilatation in relation to psychological and physical (heat, cold, blood loss, orthostasis) stress. In [25], they concluded that Finapres accuracy and precision usually suffice for reliable tracking of changes in blood pressure. Diagnostic accuracy may be achieved

with future application of corrective measures.

Tonometry is another noninvasive method used in research that, in theory, does not require an inflatable cuff [27, 28]. This method measures instantaneous BP by pressing a manometer tipped probe on an artery. The probe must flatten or applanate the artery so that its wall tension is perpendicular to the probe. However, manual and automatic applanation have proven to be difficult. Tonometric end-systolic pressure provides an estimate of effective arterial elastance(ratio of end systolic pressure to stroke volume). A measure of external left ventricular afterload. As a result, in practice, the measured waveform has been routinely calibrated with cuff BP whenever a BP change is anticipated [45]. The error range was 41 mmHg over ten calibrations. Tonometry method is not accurate enough to be used with confidence in clinical practice.

In [11], they proposed a deep recurrent neural network (RNN) consisting of multilayered Long Short-Term Memory (LSTM) networks, which are incorporated with (1) a bidirectional structure to access larger-scale context information of input sequence, and (2) residual connections to allow gradients in deep RNN to propagate more effectively. The proposed deep RNN model was tested on a static BP dataset, and it achieved root mean square error (RMSE) of 3.90 and 2.66 mmHg for systolic BP (SBP) and diastolic BP (DBP) prediction respectively. **But our proposed GRU unit achieved the RMSE of 3.86 and 3.73 for SBP and DBP respectively, in which our SBP prediction is a little better than their result reported in [11]**.

Basically the existing BP measurement methods are invasive, manual, or require a cuff. So, none are suitable for ubiquitous monitoring. Cuff use has several drawbacks. In particular, cuffs are cumbersome and time consuming to use, disruptive during ambulatory monitoring, especially while sleeping, and do not readily extend to low resources situations. To discover the convenient way to measure BP continuously and non-invasively, we still have to go through rigorous and detailed experiments and research work.

Chapter 3

Measuring Real-time Physiological Signals

For our experiments we used a BioRadio portable device from Great Lakes Neurotechnologies, Valley View, OH. BioRadio is a wireless data acquisition system capable of recording, displaying, and analyzing physiological signals in real time. Using sophisticated wireless and miniaturization technologies, the BioRadio provides physiological data acquisition that is untethered thus allowing one to move freely while monitoring physiological signals from a computer.

It is a wearable biomedical device with programmable channels for recording and transmitting combinations of human physiological signals. The BioRadio is worn by the person and is designed for acquiring physiological signals from sensors attached on the body. Physiological signals are amplified, sampled, and digitized, which can be wirelessly transmitted to a computer Bluetooth receiver and/or recorded to onboard memory for post-analysis [46].

3.1 BioRadio Configuration

The BioRadio device can be configured with a variety of sensors to acquire physiological signals. Wireless streaming and recording is done over a Bluetooth 2.4-2.484 GHz band and approximately 100 foot range. Data can simultaneously be recorded to onboard memory for post analysis. Battery charging is done over a micro-USB port and provides at least eight hours of measurement time. The four character device ID is located on the back of the unit

and can be used to identify numerous patients under observation. The BioRadio allows the synchronized real time acquisition of ECG and PPG signals which will be used to compute PTT. The synchronized data of ECG signals are measured from 5 ECG electrode leads (for ECG) located on left arm, right arm, left foot, right foot and chest and the Pulse Oximeter (for PPG) signal is measured from the left index finger (see Figure 3.1). For signal acquisition, the sampling rate is 250-16,000 Hz and the sampling resolution is 12, 16 and 24 bit [46].

Figure 3.1: BioRadio Primary Module and Sensor Pod

3.2 BioCapture Software

The BioCapture software allows the user to collect, display, save and analyze physiological data collected from the BioRadio. The intuitive design provides access to hardware configuration, data collection, review and analysis.

The BioRadio device has an built in software called the BioCapture. The BioCapture directly collects ECG and PPG signals from the sensors and exports the numerical values of the signals into an excel file and the software

directly interacts with MATLAB environment by Microsoft.NET interface.

Figure 3.2: Various physiological signal acquisition from the BioCapture Software

From the BioRadio, various synchronized physiological signals can be acquired and with the help of BioCapture software we are able to visualize and monitor those signals in real-time shown in Figure 3.2.

3.3 Measurement of Motion Data

The BioRadio's accelerometer measures gravitational force (also known as g-force) and the gyroscope measures angular velocity. Both of these sensors take measurements in three planes - x, y and z. Generally the device is attached to the patient's waist and the motion data is captured whenever the patient walks or moves from a stationary position.

For motion sensors the sampling rate is 250 Hz and the resolution is 16 bit. The accelerometer range is ± 8 g and the gyroscope range is ± -2000 °/sec [46].

Chapter 4

Calculation of Pulse Transit Time (PTT)

4.1 What is Pulse Transit Time (PTT)?

PTT is defined as the time required for the arterial pulse pressure wave to travel from the aortic valve to periphery [47]. PTT can be defined as the time between the R-peak of the electrocardiogram (ECG) signal and the peak of the photoplethysmogram (PPG) signal, when measured within the same cardiac cycle. PTT can therefore be easily measured, since only simultaneous recording of ECG and PPG are required.

Pulse transit time is defined in Figure 4.1. Physiologically, PTT represents the time delay between electrical systole in the heart (i.e., the R-wave of the ECG) and the detected peripheral pulse wave (usually measured at the finger). Electrical systole occurs just before mechanical systole, in which blood is ejected from heart through the aorta to the peripheral blood vessels [16].

4.1.1 Electrocardiogram (ECG) Signal

Electrocardiography (ECG or EKG) is the process of recording the electrical activity of the heart over a period of time using electrodes placed on the skin. The graph of voltage versus time produced by this non-invasive medical measurement technique is referred to as an electrocardiogram.

Figure 4.2 is one example of a normal ECG waveform and P, Q, R, S, T

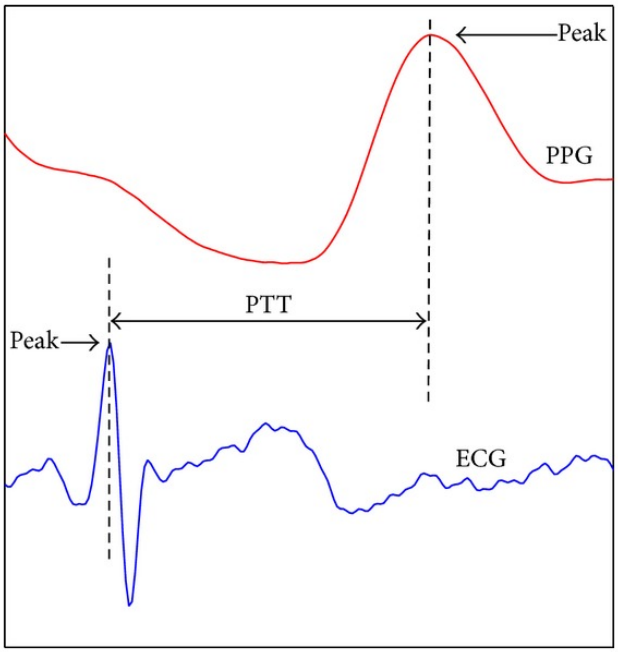

Figure 4.1: Definition of Pulse Transit Time

are the consecutive peak points.

ECG records the electrical activity of the heart at rest. It provides information about the heart rate and rhythm, and shows if there is enlargement of the heart due to high blood pressure (hypertension) or evidence of a previous heart attack (myocardial infarction). The resting ECG is different from a stress or exercise ECG or cardiac imaging test. However, the major difficulty for our application arises from the contamination of ECG signal due to motion artifacts induced by body movements in ambulatory condition [48].

4.1.2 Photoplethysmogram (PPG) Signal

A Photoplethysmogram (PPG) graph is often obtained by using a pulse oximeter which illuminates the skin and measures changes in light absorption. A PPG signal consists of an AC component and a DC component. The pulsatile portion of the PPG signal is the AC component and is obtained when light passes through the arterial blood. The DC component or non-pulsatile portion is caused the absorption of light by blood in veins, bones and tissues [49]. This signal contains important information about the heart rate variability, blood

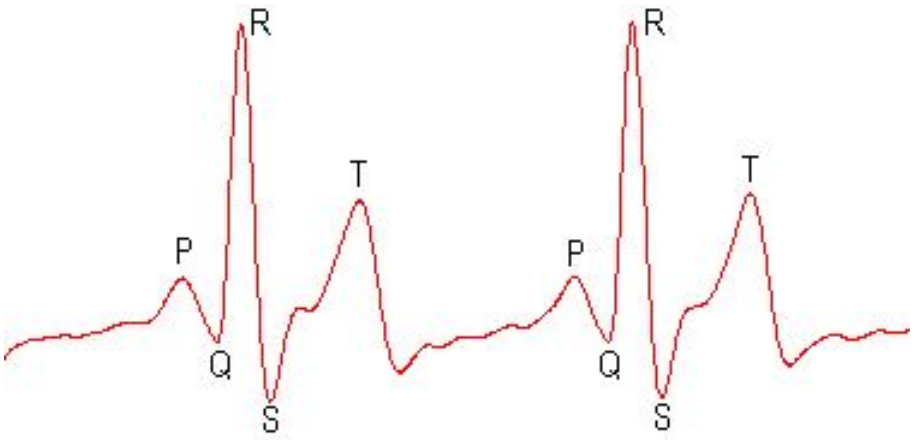

Figure 4.2: Electrocardiogram signal

pressure, respiration etc. Pulse Oximetry (PO) is the process of non-invasive way of determination of the peripheral oxygen saturation (SpO2) of blood and pulse rate, which is used to assess most basic body functions, based on the analysis of photoplethysmographical (PPG) signal pulses. This measures the volume of the blood vessel.

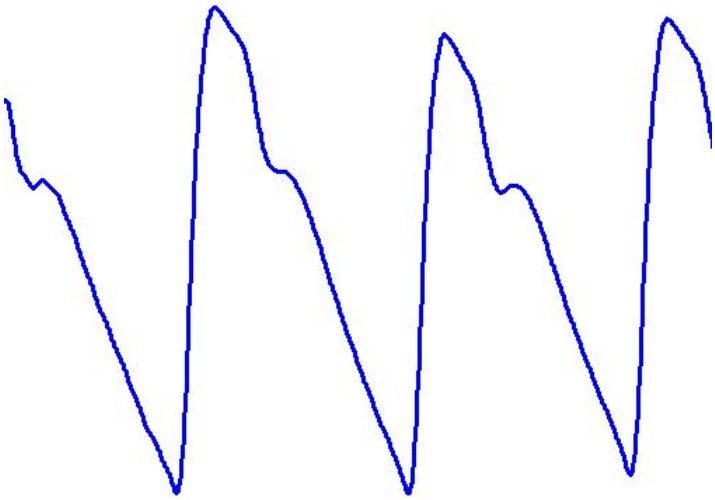

Figure 4.3: Photoplethysmogram signal

Figure 4.3 is one example of a normal PPG waveform.

Among the wide range of noise sources interfering with the PPG signal, the motion artifacts caused by patient's movements are very difficult to remove. Due to the persistent motion of the person whose PPG is measured, the signal

may be distorted and the pulsatile component is no longer identified from it. This work focuses on the removal of motion artifact from the corrupted PPG signal which enables to interpret the signal more easily and accurately.

4.2 Automated PTT Calculation

4.2.1 Processing ECG and PPG signals

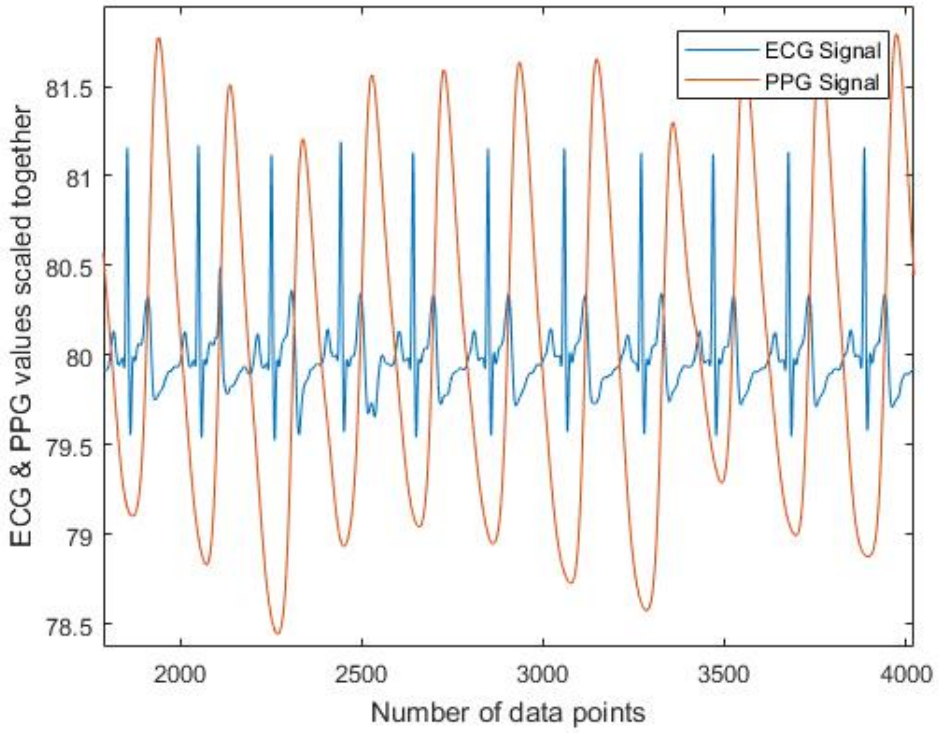

Figure 4.4: An example of clean synchronized ECG (in blue) and PPG (in red) signals

Figure 4.4 describes the synchronized, clean ECG (in blue) and PPG (in red) signals where the peaks are prominent and easily detectable. ECG is the main tool used by the physicians for identifying and interpreting the heart condition. To do so, the ECG should be free from noise and of good quality for the correct diagnosis. In real time situations ECG are corrupted by many types of artefacts. Figure 4.5 below illustrates another example of clean signals.

Different noises are affected by the ECG signal during its acquisition and transmission. Noises with high frequency include Electromyogram noise, Addi-

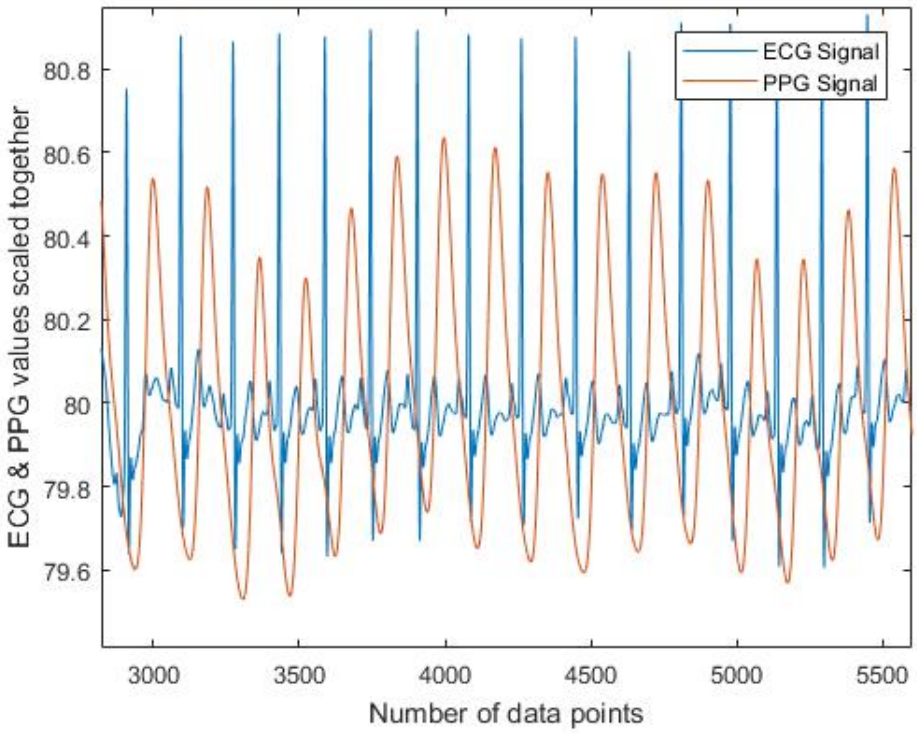

Figure 4.5: Another example of clean synchronized ECG (in blue) and PPG (in red) signals

tive white Gaussian noise, power line interference, motion artifacts. The noises contaminated in the ECG signal may lead to wrong interpretation. There is a large scientific literature on how to de-noising ECG signals and an excellent review of the state-of-the-art can be found in the book by Clifford in [50].

For ambulatory applications the dominant noise is created by motion artefacts. Motion artefacts are transient base line changes caused by changes in the electrode-skin impedance with electrode motion. As this impedance changes, the ECG amplifier sees a different source impedance which forms a voltage divider with the amplifier input impedance therefore the amplifier input voltage depends upon the source impedance which changes as the electrode position changes [51]. These include electrical interference by outside sources. During physical activity such as walking or cycling, the noise due to motion is much larger than the ECG signals.

Figure 4.6 shows one example of a noisy signal recorded during walking

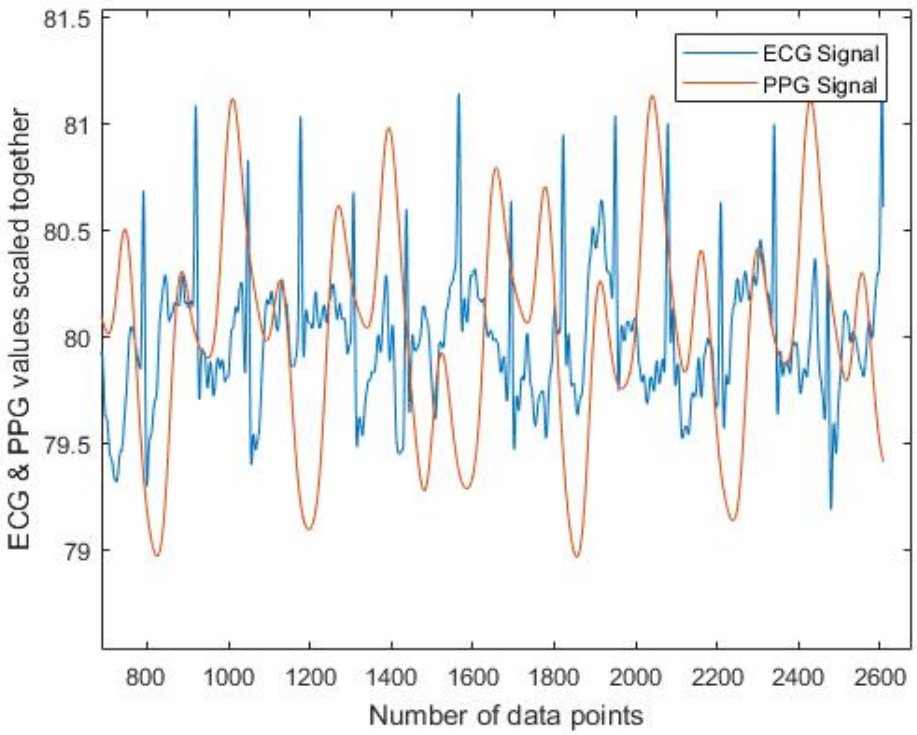

Figure 4.6: Example of a noisy ECG and PPG signal captured during walking

and Figure 4.7 shows one example of a noisy signal recorded during cycling at a normal pace.

From Figure 4.6 and Figure 4.7, one can observed that both the ECG and PPG signals were affected by motion artefacts. The corresponding peaks of both the signals are not easily distinguishable from this raw data. Artifact on the electrocardiogram can result from a variety of internal and external causes.

The motion artefact that's affecting the PPG signal seems to be a known yet unavoidable artefact. Motion artefact can significantly limit the pulse oximetry monitoring results generating frequent false alarms and loss of data. The reason for this is that during motion and low peripheral perfusion, many pulse oximeters cannot distinguish between pulsating arterial blood and moving venous blood, leading to underestimation of oxygen saturation [52].

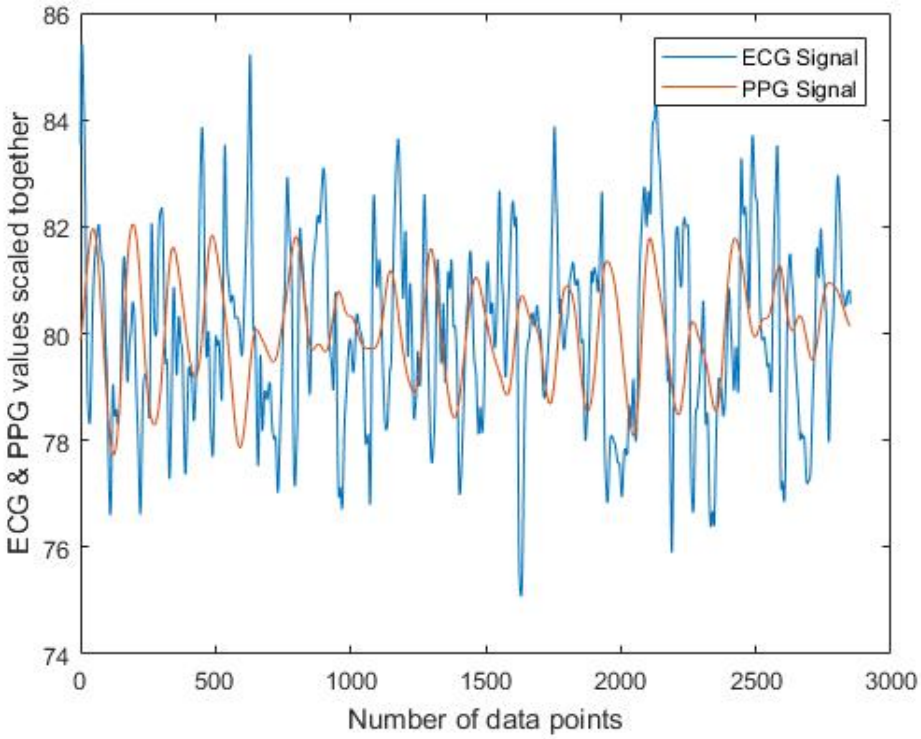

Figure 4.7: Example of a noisy ECG and PPG signal captured during cycling

4.2.2 Windowed Cross-correlation to Compute PTT

A common method for estimating the temporal dependence between events in two time series (i.e. ECG and PPG) is to use cross-correlation. Using cross-correlation, a vector or window of sequential measurement samples is selected from each time series such that both vectors contain the same number of samples. Using a Pearson correlation technique [9] one can calculate the actual correlation between the two time series over time and determine the interval of time separating the beginning of a correlated event in order to compute the lag or offset we need to measure to compute PTT.

One way to examine how the strengths and lags of association between two time series are changing over time is to use only short intervals of data from each time series to estimate the association and then select these windows so that their starting points represent increasing elapsed time from the beginning of the experiment. This has the advantage of assuming local stationarity rather than assuming stationarity over the whole time series which in most time not

true.

The cross-correlation method must be able to track changes in the time lag and strengthen the association between the two time series over the course of the experiment. Suppose we measure two variables on multiple samples separated by equal time intervals t_n. If two vectors of observations $\mathbf{X}$ and $\mathbf{Y}$ are measured and if an event measured in $\mathbf{X}$ occurs before a similar event measured in $\mathbf{Y}$, one might reason that the event in $\mathbf{X}$ may predict the event in $\mathbf{Y}$. It is also possible that an event measured in $\mathbf{Y}$ can predict an event measure in $\mathbf{X}$. Such changes in lag and strength of maximum prediction can be indicative of an underlying dynamic relationship between the constructs that gave rise to the data in measurements in $\mathbf{X}$ and $\mathbf{Y}$. The variance of the time lag and variance of strength of the cross-correlation will give estimates of two types of non-stationarity in the bivariate time series.

Within some set bounds the method should estimate the interval of time between measurement samples at which a maximum cross-correlation between the two time series occurs and the strength of that cross-correlation. Within that bounded interval of time, there may a lag between an event that occurs in time series measured by $\mathbf{X}$ and a similar event that occurs in time series measured by $\mathbf{Y}$. The method should give an estimate of the time lag between the event in $\mathbf{X}$ and the event in $\mathbf{Y}$ as well as the strength of the similarity between the two events.

Suppose we want to cross correlate two time series each containing N observations $\bar{\mathbf{X}} = \{x_1, x_2, x_3, ..., x_N\}$ and $\bar{\mathbf{Y}} = \{y_1, y_2, y_3, ..., y_N\}$ with equal sample intervals of time, Δt. If we assume stationary and choose a positive lag of τ observations, the cross-correlation between $\bar{\mathbf{X}}$ and $\bar{\mathbf{Y}}$ for a lag τ is a function of the cross-correlation r defined as:

$$r(\bar{\mathbf{X}}, \bar{\mathbf{Y}}, \tau) = \frac{1}{N-\tau} \sum_{i=1}^{N-\tau} \frac{(x_i - \bar{x})(y_i + \tau - \bar{y})}{\sigma_x \sigma_y} \tag{4.1}$$

where $\bar{x}$ and $\bar{y}$ are the means and σ_x and σ_y are the standard deviations of $\bar{\mathbf{X}}$ and $\bar{\mathbf{Y}}$ respectively. This is an ordinary Pearson correlation between the two time series with a lag of τ observations (a time interval corresponding to τ

times Δt, the sampling interval).

Using short, overlapping windows that cover the time series results in a moving estimate of correlation and lag that needs to be calculated in a way that does not favor one variable over another, since global stationarity is not assumed.

Suppose a window size w_{max} and a time lag τ on the integer interval:

$-\tau_{max} <= \tau <= \tau_{max}$ and an elapsed time index t_i from the beginning of the data. For every τ_{max} there will always be an odd number of integers in the interval. For each $t_i = \{\tau_{max} + 1, \tau_{max} + 2, ..., N - \tau_{max} - w_{max}\}$, a pair of windows $\bar{\mathbf{X}}$ and $\bar{\mathbf{Y}}$ can be selected from the data and the cross-correlation between the windows is calculated using Eqn 4.1.

The correlation is performed as following:

Step 1: Read the ECG data and the PPG data and store the values into two different arrays $\bar{\mathbf{X}}$ and $\bar{\mathbf{Y}}$;

Step 2: Perform Gaussian smoothing on the two signals with the necessary choice of the value of the smoothing parameter (i.e. the standard deviation σ_s);

Figure 4.8 describes the ECG(blue) and the PPG(red) signal after performing Gaussian smoothing to de-Noise the signal

Step 3:: Detect the maxima of the PPG signal inside a sliding window. We use the PPG as there are fewer outliers in the PPG signal than the ECG signal. By setting the other PPG values to zero, the processed PPG signal becomes very sparse. Then by performing all the operations on this sparse signal the accuracy of the method is increased. Also because of the sparsity of the signal the number of computations is reduced (i.e. the efficiency of the method increased;

In Figure 4.9 we can see the sparse PPG(red) signal only with the maxima and the ECG(blue) signal.

Step 4: Compute the sliding window correlation between the ECG and the PPG signals within each window. Cross-correlation is used to find where two signals match and also to determine the time lag between two signals. The position of the maximum value indicates the time offset at which the two

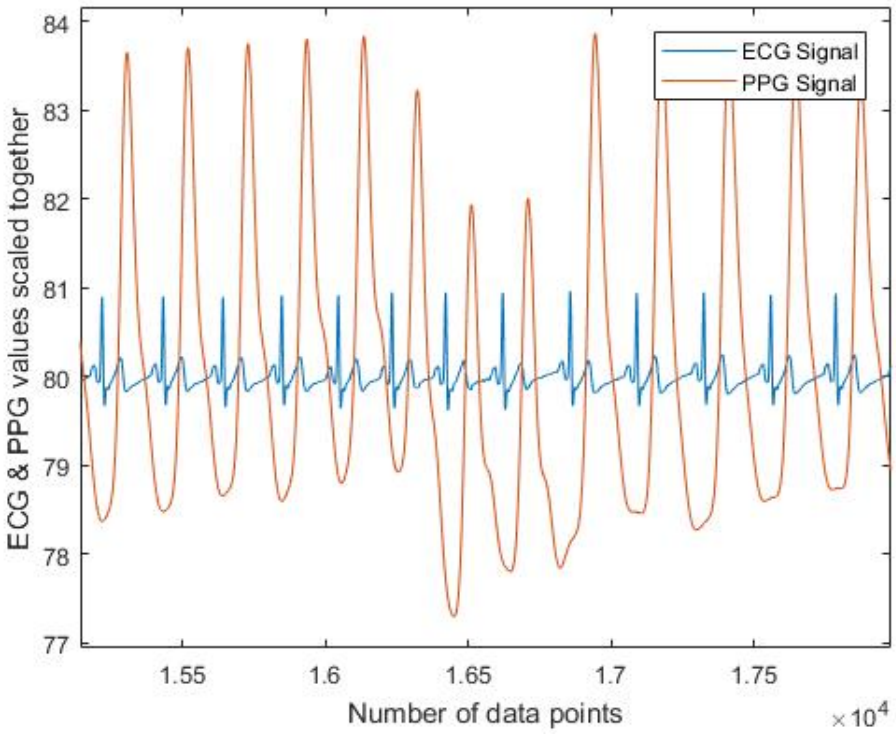

Figure 4.8: ECG(blue) and PPG(red) signals

signals are the most similar or in other words, what is the time shift between the two signals [9]. In this case the index of maximum correlation correspond to the Pulse Transit Time value we are looking for;

Step 5: Find the maximum value of cross-correlation as well as the position of the maximum correlation using a manual threshold C on the cross-correlation value;

Step 6: Store the Pulse Transit Time values into an array;

Step 7: Remove the noise in the PTT signal by using a median filter of size M where M is an odd number;

Step 8: Compare the automated and the manually computed PTT values;

Step 9: Calculate the relative percentage of error.

In Figure 4.10 one can see the graph of the correlation coefficients with the maximum correlation within a window.

To check the accuracy of the proposed method, we had to calculate the PTT values for all data sets manually to set a ground truth level. Then we

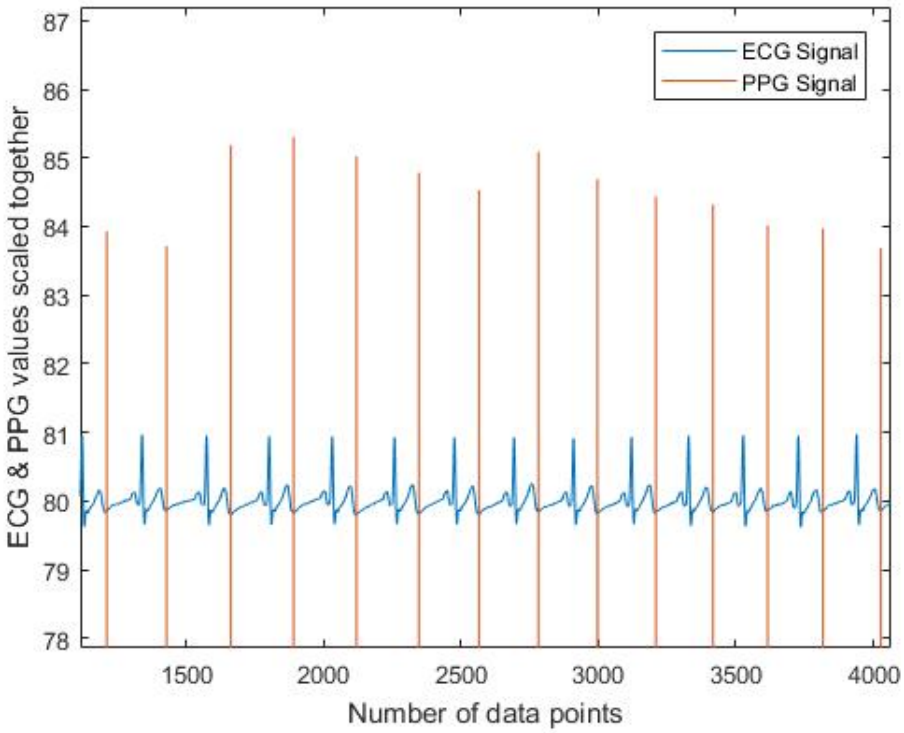

Figure 4.9: PPG signal with maxima(red) and ECG signal

compared the automated PTT values with the manually found PTT values to measure the accuracy of the method.

4.3 Evaluation of the Accuracy of the PTT Algorithm

To check the accuracy of the proposed algorithm, the PTT values were compared to a reference standard, which was defined using a manual PTT calculation (i.e. calculating the peak to peak distance of the ECG and PPG signals manually using MATLAB). The observed errors of PTT measurement were within 1% of the reference. Root-mean-squared-error (RMSE) values were calculated with and without sparsification (see Figure 4.13).

Figure 4.11 the detect peaks of the ECG signal and Figure 4.12 the detect peaks of the PPG signal manually.

We compared the automated PTT values with the manually found PTT

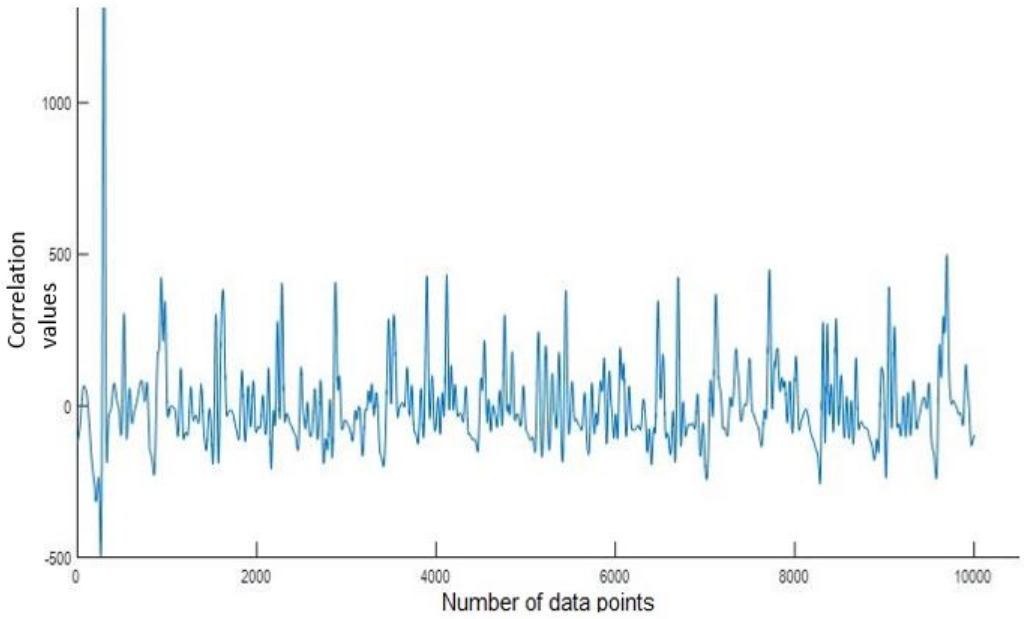

Figure 4.10: Graph of correlation coefficients in one window

values for all the data sets. Then calculated the relative percentage of error using:

$$\frac{|PTT_{automated} - PTT_{manual}| * 100}{PTT_{manual}} \tag{4.2}$$

The Mean (μ) and Standard Deviation (σ) of the error estimation were also calculated here (see Figure 4.13 and Table 4.1).

In Table 4.1, the mean relative error is around 1 % for all positions using the moving window maximum approach to calculate PTT. So the proposed algorithm with moving window maxima detection of the PPG signal to find the PTT is pretty robust.

Where as in Table 4.1 we can see the result of correlation between ECG and PPG without computing the moving window maximum of PPG signal is very poor and the mean relative error is around 6 % for all scenarios. In 4.13 the x-axis denotes the number of data points which is around 23000 when automated and manual PTT were compared.

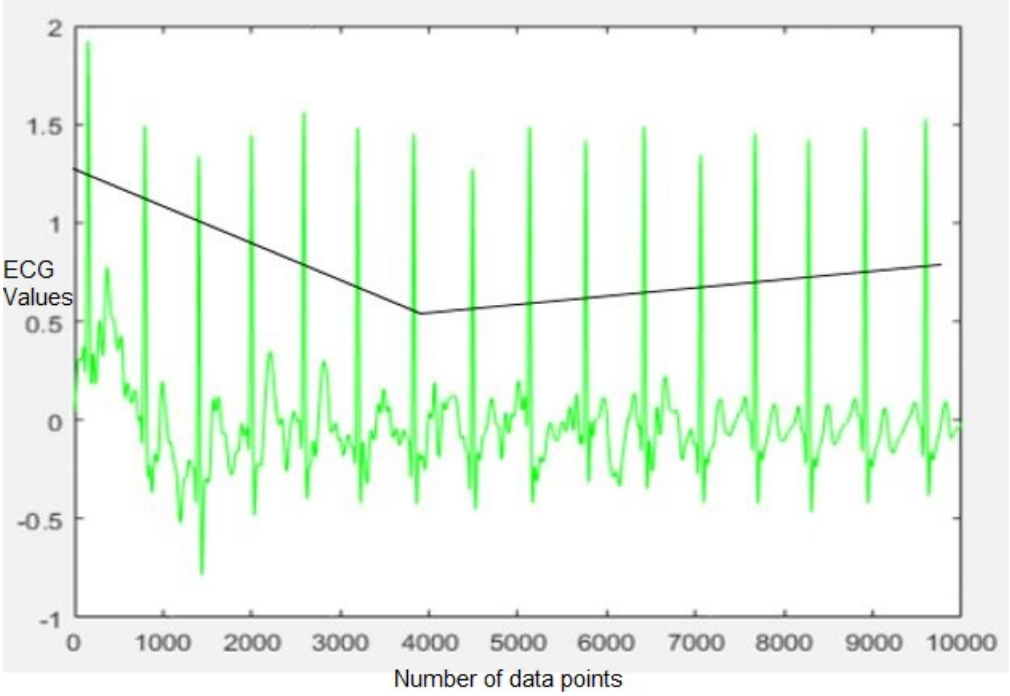

Figure 4.11: ECG signal (setting the threshold manually)

Table 4.1: Comparing the automated PTT and the manual PTT Mean ± SD of relative % error

	Using Sparsification	**Without Sparsification**
Recumbent	0.74 ± 0.49	3.06 ± 3.08
Seated	0.67 ± 0.44	4.04 ± 4.31
Standing	0.66 ± 0.43	4.97 ± 5.72
Walking	1.38 ± 1.11	8.01 ± 7.27
Cycling	1.42 ± 1.19	9.05 ± 9.18

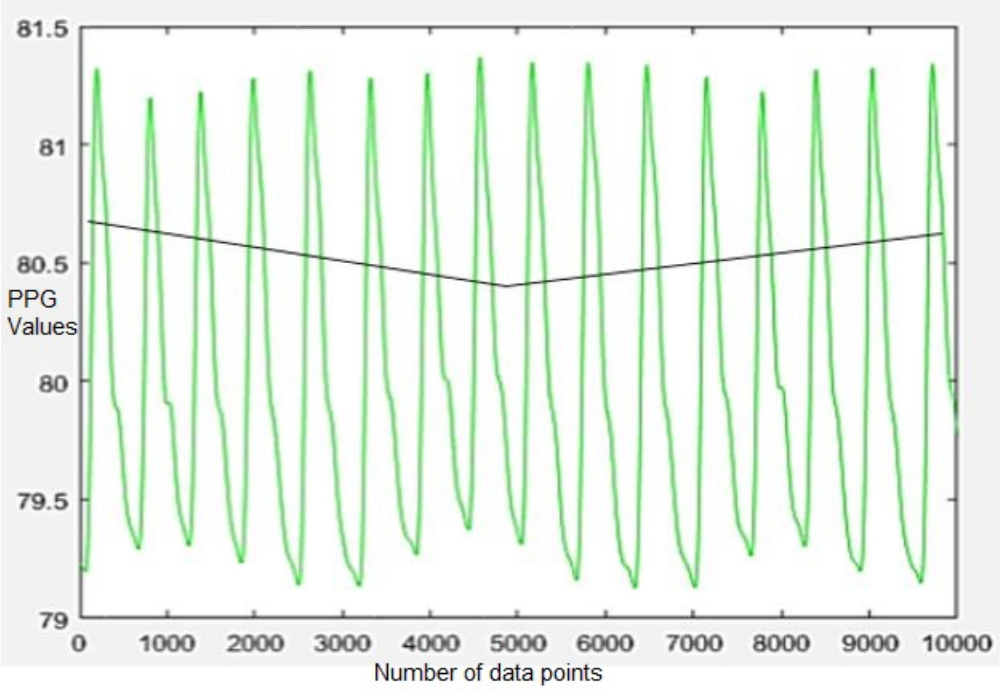

Figure 4.12: PPG signal (setting the threshold manually)

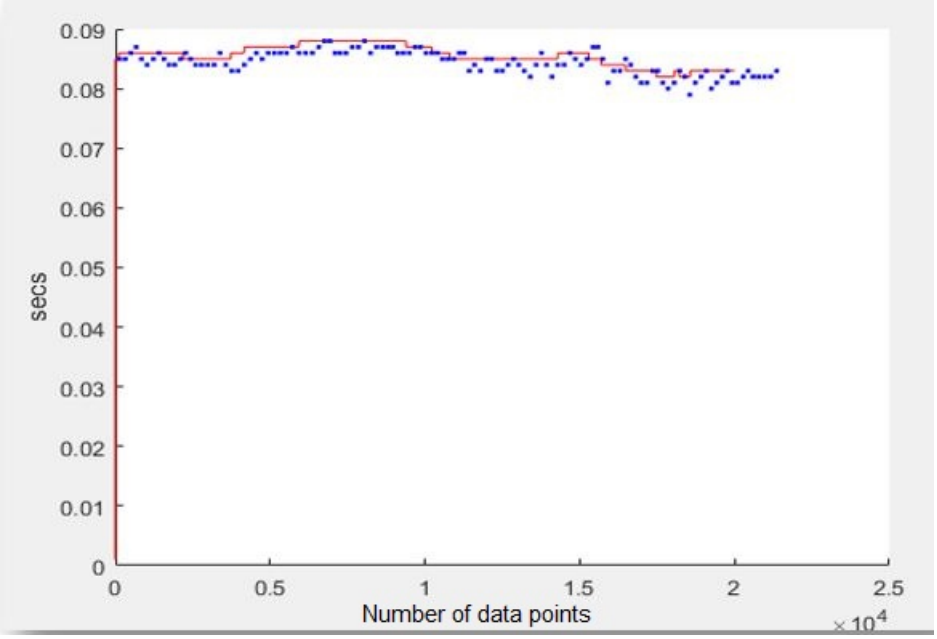

Figure 4.13: Automated PTT(red) with Manual PTT(blue)

Chapter 5

From Pulse Transit Time to Blood Pressure Measurements

Accurately converting PTT measurements to actual BP measurement is critical for the usability of this method in practice. Several calibration methods to transform PTT measurements to real BP measurements have been described in the literature [16, 8]. Most calibration methods are based on the following:

1. Define a parametric mathematical model that relates PTT measurements to BP;

2. Measure PTT and cuff-based BP from a subject in order to obtain multiple pairs of PTT and BP values;

3. Estimate the parameters of the parametric model by fitting the model to the PTT-BP measurements [18, 53, 54].

Using the parametric model to calibrate PTT measurements to diastolic, mean, and systolic of standard BP cuff measurements will allow us to measure BP of subjects without a cuff by obtaining PTT estimates and using the calibration function in real-time. This calibration function should be periodically updated to account for changes due to ageing and disease or errors in the curve.

The mathematical relationship between PTT and BP has previously been studied using physical models and empirical regression models [16, 8]. Most of

the physical models are based on the MoensKortweg and BramwellHill equations [8], using an assumed function to relate the elastic modulus to BP [8]. Some of the popular BP-PTT models will be described:

- A simple linear approximation model was proposed in [55]:

$$BP = a * PTT + b \tag{5.1}$$

  where a and b are unknown subject-specific parameters.

- Another simple model proposed by [34, 35] is based on experimental BP studies that shows that BP is inversely proportional to PTT over a wide BP range:

$$BP = \frac{a}{PTT} + b. \tag{5.2}$$

- Proneca *et al.* [56] proposed a non-linear equation to relate BP values from PTT:

$$BP = a * \ln(PTT) + b. \tag{5.3}$$

- Many of the previous simple physical models do not work asymptotically (i.e., as PTT approaches 0 or ∞). A more recent physical model capable of computing reasonable asymptotic values was proposed in [57]:

$$BP = \frac{a}{(PTT - b)^2} + c. \tag{5.4}$$

Regression models based on experimental PTT-BP data from the literature have been proposed. Many of these studies assume that PTT is related to BP via a line with a slope and intercept. However, some studies have shown that quadratic and other non-linear functions are better at predicting BP from PPT. Non-linear models including [57]) resolve the asymptotic behaviour problem and are in general more accurate overall. However, they are

generally characterized by more than two unknown parameters, which require to measure more PTT-BP pairs in order to estimate them.

Taking all possible factors into consideration and according to [8], the mathematical model described in Eqn. 5.2, is the preferred one because of its experimental validation. In order to determine the parameters a and b a straightforward least squares regression is used.

5.1 Incorporating Accelerometric and Gyroscopic Values along with PTT

- At the beginning, we used only the PTT values to calculate BP using the equation (5.2). But this linear model was not able to capture the hidden information from PTT during the motion. Here the input is

  $x = [PTTvalue]$ and the output $y = [BPvalue]$ are the scalar.

  This is the single variate regression approach.

- After that along with the PTT values and to improve the prediction during motion, we incorporated accelerometric and gyroscopic values as well in the linear model. Here the input to the model is a vector

  $x = [ECG, PPG, PTT, Accl_x, Accl_y, Accl_z, Gyro_x, Gyro_y, Gyro_z]$

  of nine elements.

  The output $y = [BPvalue]$ is a scalar.

  Accelerometric and gyroscopic values are the data from the motion sensors. This is a multivariate regression analysis.

5.2 Calibration Protocol

During the calibration process, each subject is attached to the ECG electrodes and to a pulse oximeter in a seated position. ECG and PPG data are recorded using the BioRadio system described in Chapter 3. Four cuffed BP measurements are taken after the ECG and PPG data measurements and used for calibration.

After calibration, PTT was then calculated over 20 heartbeats - 10 beats taken prior to initiating the cuffed measurement and 10 beats taken after the cuffed measurement. Measurements were performed in 5 different activity scenarios (recumbent, seated, standing, walking at a regular pace, and cycling at a comfortable pace). The proposed algorithm was used to predict BP from PTT and was compared to the actual oscillometric BP measurement for each activity conditions.

5.3 Calibration Algorithm

The algorithm for computing the calibration function between PTT and BP is the following:

- Measure the PTT and cuff BP from the subject in the rest condition i.e. the normal seated position typically used for BP measurement in clinical settings;
- Define a mathematical model between the PTT and BP in terms of (typically) two unknown parameters that depend on subject data;
- Estimate the parameters for that subject by fitting the model to the PTT-BP paired measurements.

Then subsequent BP values can be calculated for each subject from the PTT, measured under different conditions (recumbent, seated, standing, walking, cycling) and compared to the cuff-based oscillometric reference standard [7, 58].

5.4 Measurements of Pilot Study Data

5.4.1 Initial Pilot Study

For the initial study, the data were collected from 14 healthy subjects (8 women and 6 men) with no prior hypertension. The baseline characteristics of these 14 participants were as follows,

- mean age 34.4 ± 11.6 years (range 22-54), weight 75.2 ± 14.6 kg, height 173.6 ± 7.8 cm.

The training data set was collected in a seated position and the test data set with the subjects seated, lying down, standing, walking and cycling. We analyzed the five different activity levels separately. ECG and PPG signals were recorded using the BioRadio device, but the accelerometric and gyroscopic signals were not captured.

The reference standard BP was measured using a calibrated oscillometric device [59] (A&D Medical UA-651BLE).

5.4.2 Large-Scale Study

In this study, the data from 50 healthy subjects (24 men and 26 women) with no prior history of hypertension were recorded. Separate data sets for training and testing were used.

The baseline characteristics of the participants were:

- mean age 30.2 ± 11.9 years (range 18-62), weight 67.6 ± 12.5 kg, height 169.4 ± 8.7 cm, body mass index 23.5 ± 4.1 kg/m^2, and mid-arm circumference 29.0 ± 4.0 cm.

The training data set was collected with the subjects in a seated position and the test data set with the subjects seated, lying down, standing, walking and cycling. We analyzed the five different levels of activity separately. The number of data points or time steps collected during training was 60000 and the number of features was 9 (i.e. ECG, PPG, PTT, 3 Accelerometric and 3 Gyroscopic values for three axes, respectively).

The reference standard cuff-based BP was measured using a validated oscillometric device (A&D Medical UA-651BLE) [60].

5.5 Estimation of Blood Pressure Using PTT Calibration Linear Model

From the measured data sets a the parameters of the mathematical model described in (5.2) are computed.

5.5.1 The initial pilot study with 14 subjects

In this study, cuff-less, continuous BP was estimated using pulse transit time during variations in posture and activity. To show the importance of accurate PTT computation, we estimated BP with and without sparsification. Without executing the pre-processing (sparsification) of the PPG signal the acquired PTT values were not accurate. But the least square algorithm was able to predict BP with a high bias in the constants of 5.2. As a result, constant or average SBP and DBP values were obtained which is not admissible since BP varies and fluctuates minute to minute. Therefore, sparsification should be used when estimating BP using PTT.

In the following Table 5.1 and Table 5.2, Root-Mean-Squared-Error values in SBP and DBP prediction (with and without sparsification) are summarized. One can observe that there is a vast improvement in the RMSE values after performing sparsification on the PPG signal for both SBP and DBP predictions.

Table 5.1: RMSE Comparison in mmHg between measured and calculated SBP with and without sparsity.

	With Sparsity	**Without Sparsity**
Recumbent	**8.0191**	8.9083
Seated	**5.0637**	6.5119
Standing	**6.1082**	8.3313
Walking	**19.2422**	20.8162
Cycling	**17.9353**	19.1278

A Bland-Altman plots for SBP and DBP of the data are shown in Figure 5.1 and Figure 5.2. Data for 3 postures (seated, standing and walking) of all 14 subjects were plotted and the analysis reveals agreement limits of mean

Table 5.2: RMSE Comparison in mmHg between measured and calculated DBP with and without sparsity

	With Sparsity	**Without Sparsity**
Recumbent	**7.0670**	9.2466
Seated	**6.3694**	7.4087
Standing	**5.8375**	6.1547
Walking	**9.6987**	11.8634
Cycling	**10.5284**	11.8371

Table 5.3: Performance results of different positions on all subjects (Mean value ± Standard deviation)

	SBP	**DBP**
Recumbent	4.6 ± 9.6	6.64 ± 5.2
Seated	0.07 ± 5.8	-2.1 ± 7.3
Standing	0.7 ± 6.7	-4.3 ± 3.8
Walking	4.4 ± 20.9	-2.64 ± 10.4
Cycling	-10.2 ± 16.0	-3.0 ± 13.1

$\pm 1.96SD$. Limit-of-Agreement for SBP was mean $\pm 1.96SD$ that is 1.69 ± 1.96 (12.89). Limit-of-Agreement for DBP was mean $\pm 1.96SD$ that is -3.00 ± 1.96 (7.4996).

From the Bland-Altman plot analysis, it was obtained that for both SBP and DBP, only 8 out of 84 pairs of data points were located beyond the limits of $\pm 1.96SD$.

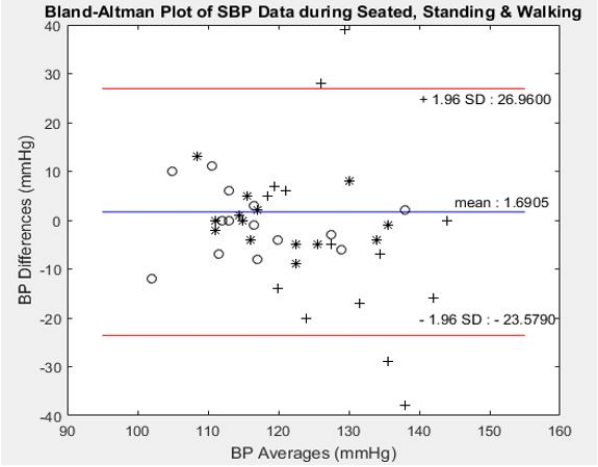

Figure 5.1: Bland-Altman plot of SBP of all 14 subjects obtained during seated (*), standing (o), walking (+).

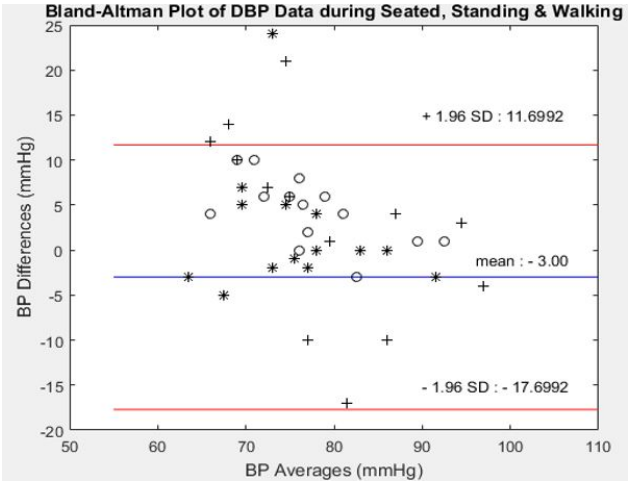

Figure 5.2: Bland-Altman plot of DBP of all 14 subjects obtained during seated (*), standing (o), walking (+).

5.5.2 Large-scale study with 50 volunteers

The results are compared for both linear model and RNN with and without accelerometric and gyroscopic values to show the impact of incorporating these motion detectors for BP prediction. Root-mean-squared-error (RMSE) values and the mean and standard deviation (SD) of error values were calculated between the reference standard and estimated systolic and diastolic BP values (SBP and DBP respectively) from both the linear and non-linear models. The following results are obtained from linear regression model. In this large scale study, multivariate linear regression model is applied by introducing the data

from motion sensors (Accelerometer and Gyroscope) along with the original signals and the feature like PTT.

Table 5.4: Comparison of RMSE values between the reference standard and estimated SBP with and without accelerometric and gyroscopic data

	With Accl. and Gyro.	**Without Accl. and Gyro.**
Recumbent	7.19	**5.74**
Seated	8.04	**5.70**
Standing	6.16	**5.14**
Walking	**7.47**	10.42
Cycling	**8.15**	11.01

Table 5.4 and Table 5.5 compare the RMSE values between the reference standard and estimated SBP and DBP with and without accelerometric and gyroscopic data. Table 5.4 the RMSE values in predicting systolic blood pressure in motionless positions (i.e. recumbent, seated and standing) are more accurate without the accelerometric and gyroscopic data. But during motion (i.e. walking and cycling) a significant amount of improvement is observed in the error estimate.

Similarly in Table 5.5 the RMSE values in predicting diastolic blood pressure in motionless positions (i.e. recumbent, seated) are more accurate without the accelerometric and gyroscopic data. But during motion (i.e. walking and cycling) again a good amount of improvement is observed in the error estimate.

Table 5.5: Comparison of RMSE values between the reference standard and estimated DBP with and without accelerometric and gyroscopic data

	With Accl. and Gyro.	**Without Accl. and Gyro.**
Recumbent	6.08	**5.22**
Seated	5.62	**4.38**
Standing	**5.90**	6.12
Walking	**7.01**	8.39
Cycling	**5.38**	7.84

In case of mean and standard deviation of error estimates in Table 5.6 and Table 5.7, a similar result is obtained. The error values in predicting SBP and DBP in motionless positions are reasonably accurate without the

Table 5.6: Comparison of Mean ± SD between the reference standard and estimated SBP with and without accelerometric and gyroscopic data

	With Accl. and Gyro.	**Without Accl. and Gyro.**
Recumbent	-0.8 ± 7.2	-0.9 ± 5.7
Seated	-1.1 ± 8.0	-0.2 ± 5.8
Standing	-0.4 ± 6.2	-0.3 ± 5.2
Walking	-2.6 ± 7.5	2.0 ± 10.3
Cycling	3.3 ± 7.5	3.3 ± 10.7

Table 5.7: Comparison of Mean ± SD between the reference standard and estimated DBP with and without accelerometric and gyroscopic data

	With Accl. and Gyro.	**Without Accl. and Gyro.**
Recumbent	-3.7 ± 4.8	-3.6 ± 3.8
Seated	2.5 ± 5.0	1.5 ± 4.2
Standing	3.3 ± 4.9	3.8 ± 4.8
Walking	1.6 ± 6.8	2.0 ± 8.2
Cycling	3.8 ± 5.1	1.8 ± 7.8

accelerometric and gyroscopic data, as there is no such presence of motion artefacts. But during motion (i.e. walking and cycling) the error is less after incorporating the motion sensors as well along with the ECG and PPG signals.

This shows the data from motion sensors actually helped our algorithm to improve the accuracy. In the following chapters, we will show that the results obtained from a recurrent neural networks are more accurate in comparison to the standard linear regression model.

Chapter 6

Estimation of Blood Pressure from Recurrent Neural Networks - LSTM case

A recurrent neural network (RNN), is a neural network model proposed in the 80's by [61] for modeling time series. The structure of the network is similar to a standard multilayer perceptron, with the distinction that it allows connections among hidden units associated with a time delay. Through these connections the model can retain information about the past, enabling it to discover temporal correlations between events that are distant in time from each other in the data. While in principle the recurrent network is a simple and powerful model, in practice, it is hard to train. Among the main reasons is the problem of *vanishing gradient* and *exploding gradient* described in [62].

Recurrent neural networks (RNNs) have recently shown significant and promising results in many machine learning tasks, especially when input and/or output are of variable length [63]. More recently [64] reported that recurrent neural networks are able to perform as well as the existing networks for machine translation.

One interesting observation, recently many of the success of neural networks were not achieved with so called "vanilla recurrent neural network" but rather with recurrent neural network with sophisticated hidden units, such as long short-term memory (LSTM) units described in [65].

One of those long short-term memory unit is a gated recurrent unit (GRU)

proposed recently in [66]. It is well established in the literature that the LSTM unit works well on sequence-based tasks with long-term dependencies.

To make a prediction model, we used RNNs, which can effectively learn the multi-timescale dependencies from a sequential time series of the PTT values. For this study, deep many-to-one and many-to-many LSTM and GRU architectures were used. These networks do not require any pre-processing of the input sequences. Thus, raw signals of the BioRadio device can be used as inputs to LSTM or GRU. The neural network is able to discover the latent correlation between different time series and learn from the dependency and predict the target values. This problem can be framed as a multivariate temporal sequence prediction problem and an appropriate application of biomedical signal processing. We used sequence-to-sequence learning framework to solve this problem as in [11].

6.1 Recurrent Neural Network Model

RNNs are the family of neural networks useful for processing temporal sequential data and have been successfully used in various sequence learning tasks to model long-term dependencies [67, 68]. In particular, the RNNs based on LSTMs can capture long range dependencies and nonlinear dynamics. LSTMs were originally introduced in [65] and subsequently, used successfully to perform supervised machine learning tasks with sequential input and output. Neural networks have been applied to medical problems and here LSTMs are applied to multivariate clinical time series prediction. One can see in Figure 6.1 and Figure 6.2 the proposed deep LSTM network for BP prediction from multiple temporal sequences. These types of data are used as the input to hidden layers in the recurrent structure. The dependency among the BP measurements will be embedded into the network structure and the RNNs can use their memory information to process sequences of inputs. RNN and its variants like LSTM are powerful dynamic systems for modelling sequential data [69]. Unlike traditional RNN, LSTM replaces the activation function of the neurons to a unit with an ingenious inner structure called LSTM [65]. LSTM

doesn't have the vanishing gradient problem and can store the memory of thousands of past discrete time steps. The following set of equations represent the process to perform parameter updates [67] in such as network:

$$f(t) = \Psi(W_{xf}x(t) + W_{hf}h(t-1) + b_f), \tag{6.1}$$

$$i(t) = \Psi(W_{xi}x(t) + W_{hi}h(t-1) + b_i), \tag{6.2}$$

$$o(t) = \Psi(W_{xo}x(t) + W_{ho}h(t-1) + b_o), \tag{6.3}$$

$$c_{in}(t) = \tanh(W_{xc}x(t) + W_{hc}h(t-1) + b_{c_{in}}), \tag{6.4}$$

$$c(t) = f(t) * c(t-1) + i(t) * c_{in}(t), \tag{6.5}$$

$$h(t) = o(t) * \tanh(c(t)), \tag{6.6}$$

where Ψ is the sigmoid function. The input, forget and the output gates are denoted by i, f, and g respectively and c_{in} is the input of the LSTM cell. tanh is the activation function of the input c_{in}.

Here the operator $*$ is the Hadamard (element-wise) product. The function $h(t-1)$ represents the previous output of the LSTM unit. In equation (6.5), the current state $c(t)$ is calculated from the previous state $c(t-1)$ and the gates in the LSTM unit. The update equation (6.6) $h(t)$ is the output of the unit at the current time point t.

Figure 6.1 shows our proposed many-to-one LSTM architecture. Here the input to the network is a vector

$x_i = [ECG, PPG, PTT, Accl_x, Accl_y, Accl_z, Gyro_x, Gyro_y, Gyro_z]$

of nine elements at each time step i.

The output $y_i = [BPvalue]$ is a scalar.

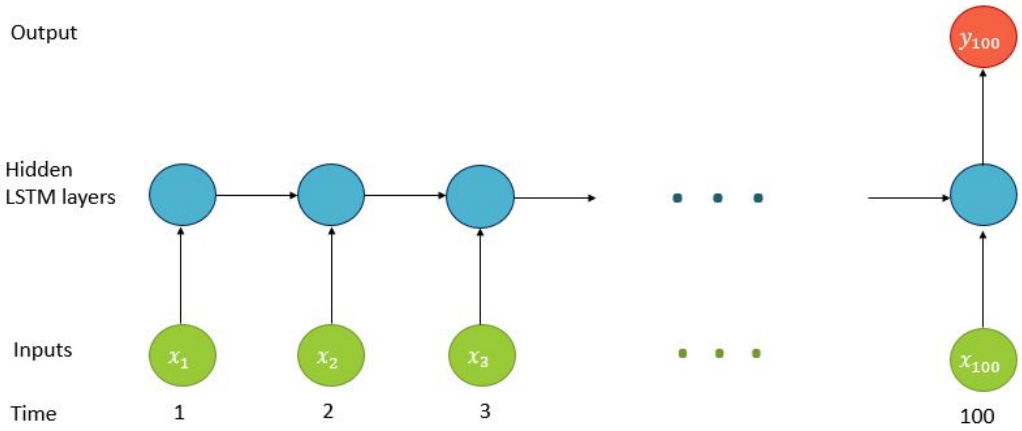

Figure 6.1: LSTM many-to-one architecture

During training every time a window of 100 time step is fed to the LSTM and the network outputs the 100th BP value in the sequence.

As another approach, we also implemented the many-to-many LSTM architecture shown in Figure 6.2. In this case, during training every time a window of 100 time step is fed to the LSTM and the network outputs corresponding sequence of 100 BP values. However, the first model i.e. the many-to-one structure performed better than the latter one (many-to-many).

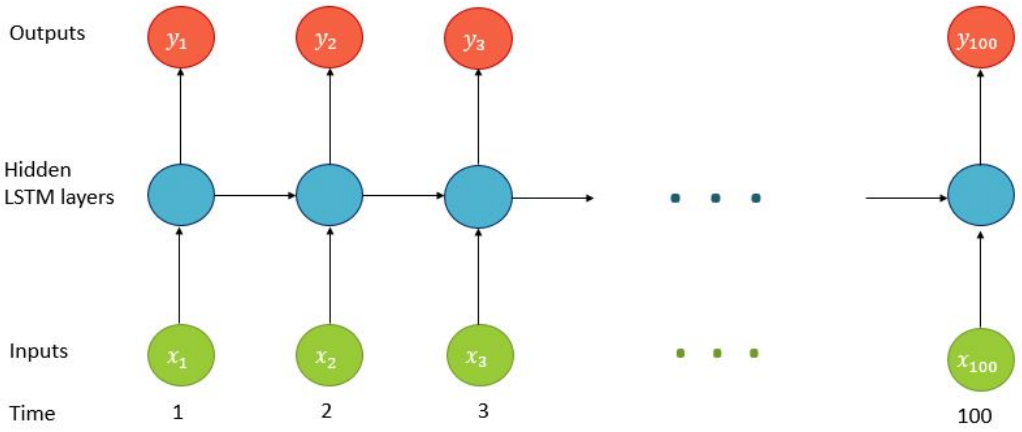

Figure 6.2: LSTM many-to-many architecture

6.2 LSTM Network Training Algorithm

We developed an LSTM layer with different numbers of neurons (32, 64, 128). In our implementation we used 32 neurons in the first hidden layer and 1 neuron in the output layer to predict BP values. The last layer is a dense layer that use mean squared error (MSE) loss function and Adam version of the stochastic gradient descent [70]. The model was trained with 50 epochs and a batch size of 64 examples with a learning rate of 0.001. All the LSTM-parameters were initialized with a uniform value distribution between -0.1 and 0.1. A dropout of 0.30 was applied to prevent over fitting. The MSE loss curves (training and validation curves) with different epochs are shown in Figure 6.4 All the experiments with the neural network were implemented using Keras API [71] with TensorFlow and on two NVIDIA GeForce GTX 1080 GPU processors. It took 1 hour to train the network. But the testing took less than 2 minutes.

The results are compared for both linear model and RNN with LSTM architecture with and without accelerometric and gyroscopic data to show the impact of incorporating these motion detectors for BP prediction. Root-mean-squared-error (RMSE) values and the mean and standard deviation (SD) of error values were calculated between the reference standard and estimated systolic and diastolic BP values (SBP and DBP respectively) from both the linear and non-linear models.

In Figure 6.3 the model summary and the details of the number of parameters used in each layer during training are described. Unlike traditional deep neural network, which uses different parameters at each layer, an RNN shares the same parameters across all steps. This reflects the fact that we are performing the same task at each step, just with different inputs. This greatly reduces the total number of parameters we need to learn.

In Figure 6.4, the loss - mean squared error vs. number of epoch curves for training (in blue) and validation (in green) are shown. Validation error decreases with training error i.e. there is no overfitting in this case.

In the following tables, the RMSE and the mean and SD of errors are

```
Layer (type)                 Output Shape              Param #
=================================================================
lstm_1 (LSTM)                (None, 32)                5376
_________________________________________________________________
dropout_1 (Dropout)          (None, 32)                0
_________________________________________________________________
dense_1 (Dense)              (None, 1)                 33
_________________________________________________________________
activation_1 (Activation)    (None, 1)                 0
=================================================================
Total params: 5,409
Trainable params: 5,409
Non-trainable params: 0
_________________________________________________________________
```

Figure 6.3: LSTM model summary and the parameters

reported using our proposed **LSTM (many-to-one) architecture**.

Table 6.1: Comparison of RMSE values between the reference standard and estimated SBP with and without accelerometric and gyroscopic data

	With Accl. and Gyro.	**Without Accl. and Gyro.**
Recumbent	**4.40**	**4.40**
Seated	**4.83**	4.92
Standing	**3.88**	4.01
Walking	**6.54**	8.05
Cycling	**7.54**	7.93

Table 6.2: Comparison of RMSE values between the reference standard and estimated DBP with and without accelerometric and gyroscopic data

	With Accl. and Gyro.	**Without Accl. and Gyro.**
Recumbent	**4.57**	4.75
Seated	**3.95**	4.18
Standing	**4.90**	5.37
Walking	**5.22**	5.35
Cycling	**4.81**	5.60

The Table 6.1 and Table 6.2 compare the RMSE values between the reference standard and estimated SBP and DBP with and without accelerometric and gyroscopic data. In case of both SBP and DBP prediction from LSTM, the results are far better using accelerometric and gyroscopic values not only

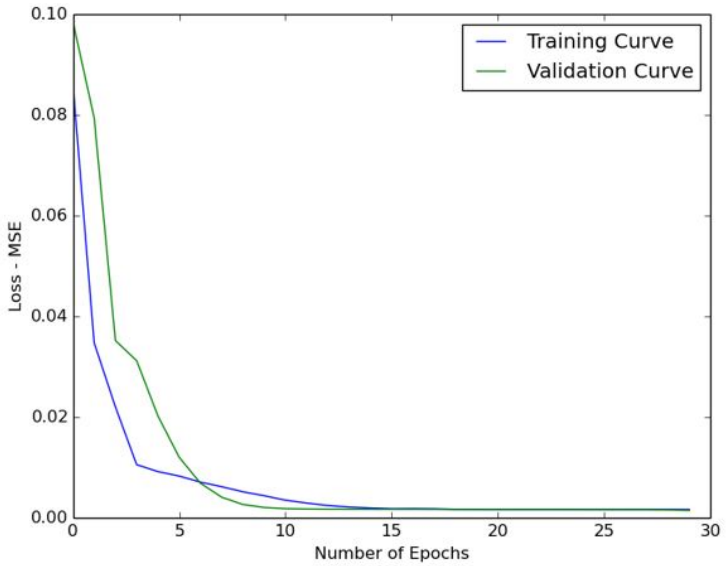

Figure 6.4: Loss - MSE vs. Epoch curve for training and validation for the LSTM

during motion (i.e. walking and cycling) but also in static positions (i.e. recumbent, seated and standing).

Table 6.3: Comparison of Mean ± SD between the reference standard and estimated SBP with and without accelerometric and gyroscopic data

	With Accl. and Gyro.	**Without Accl. and Gyro.**
Recumbent	-0.2 ± 4.2	-0.4 ± 4.4
Seated	0.02 ± 4.8	-0.5 ± 4.6
Standing	-0.2 ± 3.9	-0.3 ± 4.1
Walking	2.6 ± 6.0	2.6 ± 7.8
Cycling	2.9 ± 6.4	3.0 ± 7.8

Table 6.4: Comparison of Mean ± SD between the reference standard and estimated DBP with and without accelerometric and gyroscopic data

	With Accl. and Gyro.	**Without Accl. and Gyro.**
Recumbent	-3.2 ± 3.3	-3.4 ± 3.4
Seated	1.5 ± 3.7	1.6 ± 4.0
Standing	2.5 ± 4.2	3.5 ± 4.1
Walking	2.7 ± 4.5	2.9 ± 5.3
Cycling	2.0 ± 4.4	1.8 ± 5.8

Similarly, in case of mean and standard deviation of error estimates in Table 6.3 and Table 6.4, the same results are obtained. This shows the data from motion sensors played an important role in estimating SBP and DBP continuously from physiological signals using the proposed network.

LSTMs are better at capturing long-term dependencies than vanilla RNNs. One can think of the hidden state $h(t)$ as the memory of the network. $h(t)$ captures the information about what happened in all the previous time-steps. RNNs allow a lot of flexibility in architecture design.

Chapter 7

Estimation of Blood Pressure from Recurrent Neural Networks - GRU case

It has been observed by, Bengio *et al.* in [62] that it is quite challenging to train RNNs to capture long-term dependencies because the gradients tend to either vanish (in most of the cases) or explode (happens but rare). The *exploding gradients problem* refers to the large increase in the norm of the gradient during training. Such events are due to the explosion of the long-term components, which can grow exponentially more than short term ones. The *vanishing gradients problem* refers to the opposite behaviour, when long term components go exponentially to the value 0, making it impossible for the model to learn correlation between temporally distant events.

This makes gradient-based optimization method difficult to implement. The reasons are the variations in gradient magnitudes and the effect of short-term dependencies. Many research studies have shown how to reduce the impact of this problem by suggesting many approaches. There have been two dominant approaches to handle this problem:

One of the approaches is to devise a better learning algorithm than a simple stochastic gradient descent proposed in [72, 73], for example using the very simple clipped gradient, by which the norm of the gradient vector is clipped, or using second-order methods which may be less sensitive to the issue if the second derivatives follow the same growth pattern as the first derivatives

(which is not guaranteed to be the case).

The other approach, which is more relevant to our problem, is to design a more sophisticated activation function consisting of affine transformation followed by a simple element-wise nonlinearity by using gating units. The earliest result was a recurrent unit called LSTM proposed in [65] in 1997 and the more recent a gated recurrent unit (GRU) proposed by [66] in 2014. RNNs employing either of these recurrent units have been shown to perform well in tasks that require capturing long-term dependencies.

7.1 Gated Recurrent Unit Model

GRU was proposed to make each recurrent unit to adaptively capture dependencies of different time scales. Similarly to the LSTM unit, the GRU has gating units that modulate the flow of information inside the unit without having separate memory cells [74].

The activation of ${h_t}^j$ of the GRU at time t is a linear interpolation between the previous activation ${h_{t-1}}^j$ and the candidate activation $\tilde{{h_t}^j}$:

$$ {h_t}^j = (1 - {z_t}^j){h_{t-1}}^j + {z_t}^j \tilde{{h_t}^j} \tag{7.1} $$

where an update gate ${z_t}^j$ decides how much the unit updates its activation.

The update gate is computed by:

$$ {z_t}^j = \sigma(W_z \mathbf{x}(t) + U_z \mathbf{h}(t-1))^j. \tag{7.2} $$

By taking a linear sum between the existing state and the newly computed state is similar to the LSTM unit. The GRU, however, does not have any specific mechanism to control the degree to which its state is exposed, but exposes the whole state each time. The candidate activation $\tilde{{h_t}^j}$ is similar to the traditional recurrent unit defined in and as [64]:

$$ \tilde{{h_t}^j} = \tanh\left(W\mathbf{x}(t) + U(\mathbf{r}(t) * \mathbf{h}(t-1))\right)^j \tag{7.3} $$

where $\mathbf{r}_t$ is a set of reset gates and here the operator $*$ is the Hadamard (element-wise) product. When ${r_t}^j$ is close to 0, the reset gate effectively makes

the unit act as if it is reading the first symbol of an input sequence, allowing it to forget the previously computed state.

The reset gate ${r_t}^j$ is computed similarly to the update gate by:

$$ {r_t}^j = \sigma(W_r \mathbf{x}(t) + U_r \mathbf{h}(t-1))^j. \tag{7.4} $$

7.2 Difference Between LSTM vs GRU

The key difference between a GRU and an LSTM is that a GRU has two gates (reset and update gates) whereas an LSTM has three gates (namely input, output and forget gates). GRU is related to LSTM as both are utilizing different way if gating information to prevent vanishing gradient problem. Here are some key differences between GRU vs LSTM units:

- The GRU unit controls the flow of information like the LSTM unit, but without having to use a memory unit. It just exposes the full hidden content without any control;
- GRU is relatively new, and from my perspective, the performance is on par with LSTM, but computationally more efficient (less complex structure as pointed out);
- GRUs train faster and perform better than LSTMs on less training data if you are doing language modeling (not sure about other tasks);
- GRUs are simpler and thus easier to modify, for example adding new gates in case of additional input to the network;
- LSTMs should in theory remember longer sequences than GRUs and outperform them in tasks requiring modeling long-distance relations.

In Figure 7.1(a), i, f and o are the input, forget, and output gates respectively. The parameter c and $\tilde{c}$ denote the memory cell and the new memory

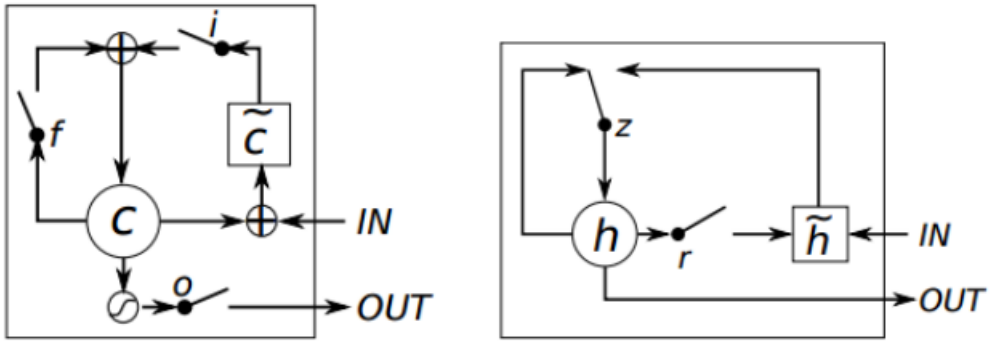

(a) Long Short-Term Memory (b) Gated Recurrent Unit

Figure 7.1: Visual representation of (a) LSTM and (b) GRU

cell content. In Figure 7.1(b), r and z are the reset and update gates and h and $\tilde{h}$ are the activation and the candidate activation functions.

7.2.1 Discussion

It is easy to notice the similarities between the LSTM unit and the GRU from Figure 7.1. The most prominent feature shared between these units is the additive component of their update from t to $t+1$, which is lacking in the traditional recurrent unit. The traditional recurrent unit always replaces the activation, or the content of a unit with a new value computed from the current input and the previous hidden state. On the other hand, both LSTM unit and GRU keep the existing content and add the new content.

This additive nature has two advantages. First, it is easy for each unit to remember the existence of a specific feature in the input stream for a long series of steps. Any important feature, decided by either the forget gate of the LSTM unit or the update gate of the GRU, will not be overwritten but be maintained as it is.

Second, and perhaps more importantly, this addition effectively creates shortcut paths that bypass multiple temporal steps. These shortcuts allow the error to be back-propagated easily without too quickly vanishing (if the gating unit is nearly saturated at 1) as a result of passing through multiple, bounded non-linearities, thus reducing the difficulty due to vanishing gradients

[75]. These two units however have a number of differences as well. One feature of the LSTM unit that is missing from the GRU is the controlled exposure of the memory content. In the LSTM unit, the amount of the memory content that is seen, or used by other units in the network is controlled by the output gate. On the other hand the GRU exposes its full content without any control.

Another difference is in the location of the input gate, or the corresponding reset gate. The LSTM unit computes the new memory content without any separate control of the amount of information flowing from the previous time step. Rather, the LSTM unit controls the amount of the new memory content being added to the memory cell independently from the forget gate. On the other hand, the GRU controls the information flow from the previous activation when computing the new, candidate activation, but does not independently control the amount of the candidate activation being added (the control is tied via the update gate). From these similarities and differences alone, it is difficult to conclude which types of gating units would perform better in general. Although [64] reported that these two units performed comparably to each other according to their preliminary experiments on machine translation, it is unclear whether this applies as well to tasks other than machine translation.

7.3 GRU Network Algorithm

We created our GRU layer with different numbers of neurons (4, 8, 16) and it performed comparatively well with 4 neurons in the first hidden layer and 1 neuron in the output layer to predict BP values. The last layer is a dense layer and we used mean squared error (MSE) loss function and Adam version of the stochastic gradient descent [70]. The model was trained with 50 epochs and a batch size of 64 examples with learning rate of 0.001. All the GRU-parameters were initialized with the uniform distribution between -0.1 and 0.1. A dropout of 0.30 was applied to prevent overfitting. The MSE loss curves (training and validation curves) with different epochs are shown in figure 7.2. Validation error decreases with training error i.e. there is no overfitting in this case. All

the experiments with the neural network were implemented using Keras API [71] with TensorFlow and on a double NVIDIA GeForce GTX 1080. It took 45 minutes to train the network. But the testing took less than 2 minutes.

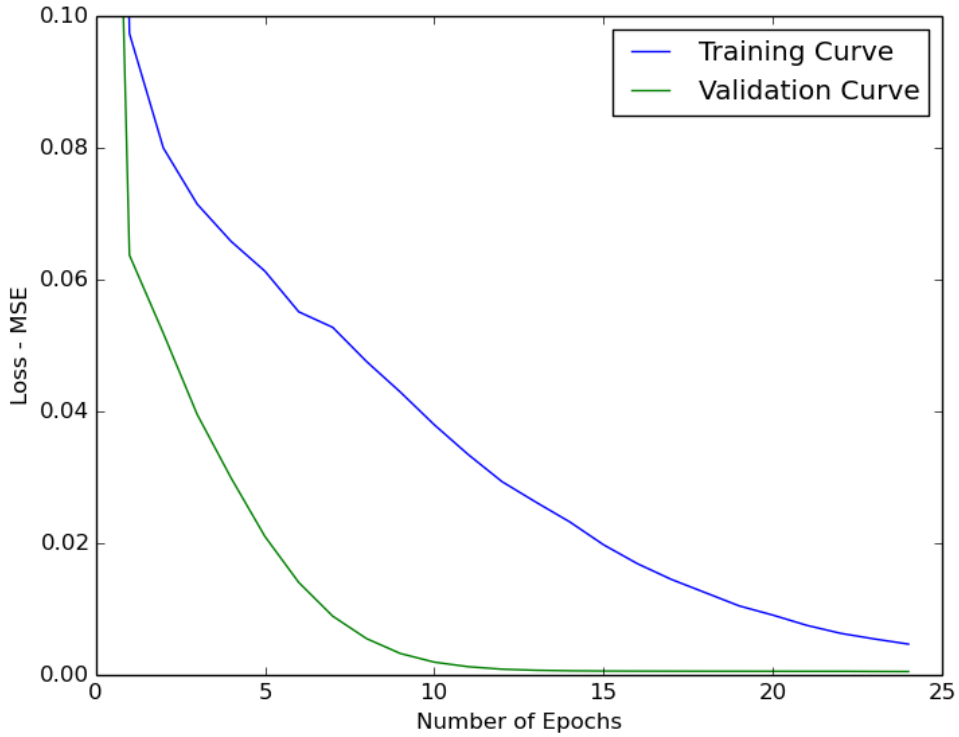

Figure 7.2: Loss - MSE vs. Epoch curve for training and validation for the GRU

In the following tables, the RMSE and the mean and SD of errors are reported using the proposed **GRU (many-to-one) architecture**.

The Table 7.1 and Table 7.2 compare the RMSE values between the reference standard and estimated SBP and DBP with and without accelerometric and gyroscopic data. Similar to LSTM, SBP and DBP prediction from GRU results are far better using accelerometric and gyroscopic values not only during motion (i.e. walking and cycling) but also in static positions (i.e. recumbent, seated and standing).

One can see the mean and standard deviation of error estimates in Table 7.3 and Table 7.4 where the results are similar. This shows the data from motion sensors played an important part in estimating SBP and DBP continuously

Table 7.1: Comparison of RMSE values between the reference standard and estimated SBP with and without accelerometric and gyroscopic data

	With Accl. and Gyro.	**Without Accl. and Gyro.**
Recumbent	**3.86**	4.16
Seated	**4.22**	4.24
Standing	**3.34**	3.68
Walking	**6.10**	7.44
Cycling	**6.64**	7.12

Table 7.2: Comparison of RMSE values between the reference standard and estimated DBP with and without accelerometric and gyroscopic data

	With Accl. and Gyro.	**Without Accl. and Gyro.**
Recumbent	**3.96**	4.39
Seated	**3.73**	3.86
Standing	**4.40**	4.62
Walking	**4.80**	4.95
Cycling	**4.44**	4.86

Table 7.3: Comparison of Mean ± SD between the reference standard and estimated SBP with and without accelerometric and gyroscopic data

	With Accl. and Gyro.	**Without Accl. and Gyro.**
Recumbent	0.2 ± 3.9	-0.5 ± 4.2
Seated	0.08 ± 4.5	-0.4 ± 4.3
Standing	-0.2 ± 3.4	-0.3 ± 3.7
Walking	2.3 ± 5.7	2.4 ± 7.2
Cycling	3.8 ± 5.0	1.5 ± 7.1

Table 7.4: Comparison of Mean ± SD between the reference standard and estimated DBP with and without accelerometric and gyroscopic data

	With Accl. and Gyro.	**Without Accl. and Gyro.**
Recumbent	-2.7 ± 3.0	-3.1 ± 3.2
Seated	1.7 ± 3.4	1.4 ± 3.6
Standing	2.4 ± 3.8	3.0 ± 4.10
Walking	2.5 ± 4.2	1.4 ± 5.0
Cycling	1.8 ± 4.1	1.4 ± 4.8

from physiological signals using deep learning techniques.

Chapter 8

Conclusion

8.1 Discussion

In this study, cuff-less, continuous BP was estimated using pulse transit time during variations in posture and activity. To show the importance of accurate PTT computation, we estimated BP with and without sparsification. Without executing the pre-processing (sparsification) of the PPG signal the acquired PTT values were not accurate. But the least square algorithm was able to predict BP with a high bias. As a result, constant or average SBP and DBP values were obtained which is not admissible since BP varies and fluctuates minute to minute. Therefore, sparsification should be used when estimating BP using PTT. This pre-processing increased the accuracy and efficiency (computational time) of our proposed method.

The linear regression model predicted the BP from PTT comparatively better during recumbent, seated and standing positions. However, walking and cycling introduce baseline noise into both the ECG and PPG signals, making it more difficult to accurately determine ECG signals from the heart as opposed to the one created by the motion. This limits the accurate BP estimation. If we consider a difference between the experimental BP measurement and reference standard of less than 5 ± 8 mmHg as indication of acceptable accuracy [76], then the PTT-based estimation in this study appears sufficiently accurate if one is seated or standing but not for other activities.

To improve the BP estimation in all posture and activity, we applied deep learning based approach as we collected a reasonably large dataset from 50

healthy volunteers as deep learning needs a lot of data to train the model. As the problem is multidimensional time series prediction problem, we implemented RNN models (specifically many-to-many and many-to-one LSTM and GRU) that can predict continuous BP sequences from physiological signals such as ECG, PPG but also motion sensors like accelerometers and gyroscopes. The captured signals in the seated or standing positions are relatively comparable to oscillometric BP; however, walking and cycling introduce baseline noise into both the ECG and PPG signals and have varying physiological states from resting, making it more difficult to accurately estimate the corresponding BP values. To predict BP more accurately during activity, the accelerometric and gyroscopic values were used to compensate for motion artefact. The BioRadio's accelerometer measures gravitational force (also known as g-force) and the gyroscope measures angular velocity. Both of these sensors take measurements in three planes - x, y, and z directions. The motion artifacts that affect the ECG and PPG signals are a known, yet unavoidable issue caused by activity.

The training dataset was collected with the subjects in a seated position and the test dataset with the subjects seated, lying down, standing, walking and cycling. As we trained the models on the data collected in motionless condition, it is expected that the model should perform well on the test data from seated, recumbent and standing positions. But we also have test data collected during motion (i.e. while walking and cycling) which the model did not see during training. This problem is called an **extrapolation problem** and deep learning or any other algorithm has not offered any solution for the extrapolation problem [77]. Also, as BP values vary tremendously from person to person, we had to train the network for each subject, that means we needed to calibrate the system for each person.

However after including accelerometric and gyroscopic data, we achieve significant increase in the accuracy for all positions specially during motion by using RNNs. The mean $\pm$ standard deviation is 0.08 ± 4.5 for SBP and 1.7 ± 3.4 for DBP in seated position and 2.3 ± 5.7 for SBP and 2.5 ± 4.2 for DBP while walking which is permissible according to the accepted threshold

for accuracy using GRUs. Also, the root mean squared error between the reference standard and estimated SBP and DBP are 4.22 and 3.73 respectively for motionless position and are 6.10 and 4.80 for walking in case of GRUs.

Between LSTM and GRU, although the achieved accuracy are very similar, GRU performed slightly better than LSTM in all contexts. It can be stated that the difference between the estimated BP from RNN and the reference standard was less than the accepted threshold in all five scenarios. We demonstrated that modeling the temporal dependency in BP dynamics can significantly improve long term BP prediction accuracy, which is one of the most challenging problems in cuffless BP estimation. We proposed a novel deep RNN with LSTM and GRU to tackle this challenge. The experimental results show that the deep RNN model achieves the state-of-the-art accuracy for static as well as during motion for continuous BP prediction.

The deep learning based method applied in this study appears sufficiently accurate not only in motionless conditions (recumbent, seated, standing) but also for walking and cycling, where motion artifacts are present. If we have a large labeled dataset, deep learning works great in that case. This novel approach has a significant potential contribution in BP measurement in different postures and activity for hypertension control and management.

8.2 Future Work

In the future, the current model should be further developed such that it learns the multi-scale dependency more accurately and performs multi-tasking by predicting SBP, DBP and mean blood pressure (MBP) in parallel. Such auxiliary training could be applied during training phase and could improve the overall performance and accuracy. Also, if we can build a system that is generic for all individual, that would revolutionize hypertension diagnosis and management. However this is still an open problem to come up with a machine that will automatically predict blood pressure from a few other parameters where no calibration is needed prior to this.

Bibliography

[1] Lim SS, Vos T, Flaxman AD, Goodarz D, Shibuya K, Adair-Rohani H, and Al-Mazroa MA et al. A comparative risk assessment of burden of disease and injury attributable to 67 risk factors and risk factor clusters in 21 regions, 1990-2010: A systematic analysis for the global burden of disease study 2010. *The Lancet*, 380(9859):2224–2260, 2012.

[2] V. L. Burt et al. Prevalence of hypertension in the us adult population: Results from the third national health and nutrition examination survey, 1988-1991. *Hypertension*, 25:305–313, 1995.

[3] Heather Ting Ma. A blood pressure monitoring method for stroke management. *BioMed Research International*, 2014(571623):7 pages, 2014.

[4] H. Gesche et al. Continuous blood pressure measurement by using the pulse transit time: Comparison to a cuff-based method. *Springer-Verlag*, 2011.

[5] X. H. Fang et al. Longitudinal study of blood pressure and stroke in over 37,000 people in China. *Cerebrovascular Diseases*, 11(3):225–229, 2001.

[6] P. W. Wilson et al. Prediction of coronary heart disease using risk factor categories. *Circulation*, 97(18):1837–1847, 1998.

[7] T. Wibmer et. al. Pulse transit time and blood pressure during cardiopulmonary exercise tests. *Physiological Research, Institute of Physiology, Academy of Sciences of the Czech Republic, Prague, Czech Republic*, 63(ISSN 0862-8408):287–269, 2014.

[8] Ramakrishna Mukkamala (member IEEE) et. al. Toward ubiquitous blood pressure monitoring via pulse transit time: Theory and practice. *IEEE Transactions On Biomedical Engineering*, 62(8), 2015.

[9] J. L. Rotondo K. King S. M. Boker, M. Xu. Windowed crosscorrelation and peak picking for the analysis of variability in the association between behavioral time series. *Psychological Methods*, 7(3):338–355, 2002.

[10] Che-Chang Yang and Yeh-Liang Hsu. A review of accelerometry-based wearable motion detectors for physical activity monitoring. *Sensors 2010, 7772-7778, ISSN 1424-8220*, 2010.

[11] Peng Su et. al. Long-term blood pressure prediction with deep recurrent neural networks. *arXiv:1705.04524*, 2018.

[12] K. G. Ng and C. F. Small. Survey of automated noninvasive blood pressure monitors. *J. Clin. Eng.*, 19:452–487, 1994.

[13] A. P. Avolio M. F. O'Rourke R. P. Kelly, C. S. Hayward. Noninvasive determination of age-related changes in the human arterial pulse. *Circulation*, 80:1652–1659, 1989.

[14] Ko S. Choi Y, Zhang Q. Noninvasive cuffless blood pressure estimation using pulse transit time and hilberthuang transform. *Comput Electr Eng*, 39:103–111, 2012.

[15] Joharinia S. Younessi Heravi MA, Khalilzadeh MA. Continous and cuffless blood pressure monitoring using ECG and SpO2 signals. *J Biomed Phys Eng*, 4(1):27–32, 2014.

[16] M. Cerny L. Peter, N. Noury. A review of methods for non-invasive and continuous blood pressure monitoring: Pulse transit time method is promising? *Published in IRBM journal*, 35:271282, 2014.

[17] Ichikawa S. Takeuchi Y. Togawa T. Chen M.W., Kobayashi T. Continuous estimation of systolic blood pressure using the pulse arrival time and intermittent calibration. *MedBiol Eng Comput*, 28(5):569574, 2000.

[18] C. C. Y. Poon and Y. T. Zhang. Cuff-less and noninvasive measurements of arterial blood pressure by pulse transit time. *in Proceedings of the 27th Annual International Conference of the Engineering in Medicine and Biology Society (IEEE-EMBS 05)*, page 58775880, 2005.

[19] Y.-T. Zhang X.-R. Ding X. Hong Q. He F. Miao, N. Fu and Y. Li. A novel continuous blood pressure estimation approach based on data mining techniques. *IEEE Journal of Biomedical and Health Informatics*, 2017.

[20] S. Deb M. Jain, N. Kumar and A. Majumdar. A sparse regression based approach for cuff-less blood pressure measurement. *Acoustics, Speech and Signal Processing (ICASSP), IEEE International Conference on*, page 789793, 2016.

[21] S. S. Thomas et al. Biowatch: A non-invasive wrist-based blood pressure monitor that incorporates training techniques for posture and subject variability. *IEEE Journal of Biomedical and Health Informatics*, 2015.

[22] K. Ivanov et al. He Liu. Toward a smartphone application for estimation of pulse transit time. *Sensors*, (ISSN 1424-8220), 2015.

[23] Hao Lin et.al. Noninvasive and continuous blood pressure monitoring using wearable body sensor networks. *IEEE Computer Society*, 2015.

[24] P. Sridhar S. Ilango. A non-invasive blood pressure measurement using android smart phones. *IOSR Journal of Dental and Medical Sciences*, 13(ISSN 1424-8220):28–31, 2014.

[25] B. P. M. Imholz et al. Fifteen years experience with finger arterial pressure monitoring. *Cardiovasc. Res.*, 38:605616, 1998.

[26] K. H. Wesseling et al. Physiocal, calibrating finger vascular physiology for finapres. *Homeostasis*, 36:6782, 1995.

[27] G. M. Drzewiecki et al. Deformational forces in arterial tonometry. *New York, NY, USA: IEEE Press*, 28:642645, 1984.

[28] J. S. Eckerle. *Tonometry arterial*. Encyclopedia of Medical Devices and Instrumentation, J. G. Webster, Ed. New York, NY, USA: Wiley, 1988.

[29] F. Fischer N. Lutter, H.G. Engl and R.D. Bauer. Noninvasive continuous blood pressure control by pulse wave velocity. *Zeitschrift fur Kardiologie*, 85(3):124126, 1996.

[30] D. M. Davidson M. A.Winchester R. A. Allen, J. A. Schneider and C. B. Taylor. The covariation of blood pressure and pulse transit time in hypertensive patients. *Psychophysiology*, 18(3):301306, 1981.

[31] D. Shapiro E. Rubenstein J. D. Lane, L. Greenstadt and D. James. Pulse transit time and blood pressure: An intensive analysis. *Psychophysiology*, 20(1):45–49, 1983.

[32] D. J. Pitson and J. R. Stradling. Value of beat-to-beat blood pressure changes, detected by pulse transit time, in the management of the obstructive sleep apnoea/hypopnoea syndrome. *European Respiratory Journal*, 12(3):685692, 1998.

[33] S. I. Yagi T. Asakawa T. Kawasaki, S. Sasayama and T. Hirai. Noninvasive assessment of the age related changes in stiffness of major branches of the human arteries. *Cardiovascular Research*, 21(9):678687, 1987.

[34] L. Geddes et al. Pulse transit time as an indicator of arterial blood pressure. *Psychophysiology*, 18:7174, 1981.

[35] G. Zhang et al. Pulse arrival time is not an adequate surrogate for pulse transit time as a marker of blood pressure. *J. Appl. Physiology*, 111:16811686, 2011.

[36] D. J.Webb R. A. Payne, C. N. Symeonides and S. R. J.Maxwell. Pulse transit time measured from the ECG: An unreliable marker of beat-to-beat blood pressure. *Journal of Applied Physiology*, 100(1):136141, 2006.

[37] J. van Jones G. V. Marie, C. R. Lo and D. W. Johnston. The relationship between arterial blood pressure and pulse transit time during dynamic and static exercise. *Psychophysiology*, 21(5):521527, 1984.

[38] C. C. Y. Poon Y. L. Zheng and Y. T. Zhang. Investigation of temporal relationship between cardiovascular variables for cuffless blood pressure estimation. *in Proceedings of the IEEEEMBS International Conference on Biomedical and Health Informatics (BHI 12)*, page 644646, 2012.

[39] Murray A. Zheng D. Non-invasive quantification of peripheral arterial volume distensibility and its non-linear relationship with arterial pressure. *J Biomech*, 42(8):1032–7, 2009.

[40] Younessi Heravi et.al. A new approach for blood pressure monitoring based on ECG and PPG signals by using artificial neural networks. *International Journal of Computer Applications (0975 8887)*, 103(12):36–40, 2014.

[41] B. H. McGhee and E. J. Bridges. Monitoring arterial blood pressure: What you may not know. *Crit. Care Nurse*, 22:60–79, 2002.

[42] D. Perloff et al. Human blood pressure determination by sphygmomanometry. *Circulation*, 88:24602470, 1993.

[43] G. Drzewiecki et al. Theory of the oscillometric maximum and the systolic and diastolic detection ratios. *Ann. Biomed. Eng.*, 22:8896, 1994.

[44] B. S. Alpert et al. Oscillometric blood pressure: A review for clinicians. *J. Am. Soc. Hypertension*, 8:930938, 2014.

[45] S. Hansen and M. Staber. Oscillometric blood pressure measurement used for calibration of the arterial tonometry method contributes significantly to error. *Eur. J. Anaesthesiol.*, 23:781787, 2006.

[46] BioRadio. Great lakes neurotechnologies, valley view, oh. *https://glneurotech.com/bioradio/bioradio-specifications/*.

[47] Smith R.P. et.al. Pulse transit time: an appraisal of potential clinical applications. *Thorax*, 54:452–457, 1999.

[48] Tanmay Pawar et.al. Impact analysis of body movement in ambulatory ecg. *Proceedings of the 29th Annual International Conference of the IEEE EMBS*, 2007.

[49] M. K. Diab. Masimo Corporation. Plethysmograph pulse recognition processor. *U.S. Patent Application, US 044,918 B2*, 2006.

[50] Patrick E. McSharry Gari D. Clifford, Francisco Azuaje. Advanced methods and tools for ecg data analysis. *Artech House Publishers*, 2006.

[51] Manal Afify Jadallah Standford L. Yates Stephen R.Quint H.Troy N Nagle Gary M, Friesen Thomas C. Jannett. A comparision of the noise sensitivity of nine qrs detection algorithms. *IEEE Transactions on Biomedical Engineering*, 37(1), 1990.

[52] Barker S J. Motion resistant pulse oximetry: A comparison of new and old models. *Anesth Analg.*, 95(4):967972, 2002.

[53] D. J. Hughes et. al. Measurements of youngs modulus of elasticity of the canine aorta with ultrasound. *Ultrasonic Imag.*, 1:356367, 1979.

[54] B. Gribbin et. al. Pulse wave velocity as a measure of blood pressure change. *Psychophysiology*, 13:8690, 1976.

[55] Qin Y Pan W Yu M Xiang H, Liu Y. Calibration of pulse wave transit time method in blood pressure measurement based on the korotkoff sound delay time. *World Congress on Medical Physics and Biomedical Engineering*, page 4269, 2012.

[56] Aubert X Carvalho P Proenca J, Muehlsteff J. Is pulse transit time a good indicator of blood pressure changes during short physical exercise in a young population? *Engineering in Medicine and Biology Society (EMBC)*, page 598601, 2010.

[57] S. S. Thomas et. al. Biowatch 2014; a wrist watch based signal acquisition system for physiological signals including blood pressure. *in Proc. IEEE 36th Annu. Int. Conf. Eng. Med. Biol. Soc.*, page 22862289, 2014.

[58] M. H. Moradi S. Mottaghi and L. Roohisefat. Cuff less blood pressure estimation during exercise stress test. *International Journal of Bioscience, Biochemistry and Bioinformatics*, 2(6), 2012.

[59] Protogerou A Nasothimiou E Kapralos C Stergiou GS, Tzamouranis D. Validation of the Microlife Watch BP Office professional device for office blood pressure measurement according to the international protocol. *Blood Press Monit. 2008*, 13:299–303, 2008.

[60] Claudio Fania Elisabetta Benetti and Paolo Palatini. Validation of the A-D BP UA-651 device for home blood pressure measurement according to the european society of hypertension international protocol revision 2010. *Blood Press Monit. 2014*, 19(1):50–3, 2014.

[61] Hinton G. E. Rumelhart D. E. and Williams R. J. Learning representations by back- propagating errors. *Nature*, 323(6088):533536, 1986.

[62] P. Simard Y. Bengio and P. Frasconi. Learning long-term dependencies with gradient descent is difficult. *IEEE Transactions on Neural Networks*, 5(2):157166, 1994.

[63] A. Graves. Supervised sequence labelling with recurrent neural networks. *Studies in Computational Intelligence. Springer*, 2012.

[64] K. Cho D. Bahdanau and Y. Bengio. Neural machine translation by jointly learning to align and translate. *Technical report, arXiv preprint arXiv:1409.0473*, 2014.

[65] S. Hochreiter and J. Schmidhuber. Long short-term memory. *Neural Computation*, 9(8):17351780, 1997.

[66] D. Bahdanau K. Cho, B. van Merrienboer and Y. Bengio. On the properties of neural machine translation: Encoder-decoder approaches. *arXiv preprint arXiv:1409.1259*, 2014.

[67] Geoffrey E Hinton David E Rumelhart and Ronald J Williams. Learning internal representations by error propagation. *Technical report, DTIC Document*, 1985.

[68] Andrej Karpathy and Li Fei-Fei. Deep visual-semantic alignments for generating image descriptions. *In IEEE Conference on Computer Vision and Pattern Recognition (CVPR)*, page 31283137, 2015.

[69] Yoshua Bengio Yann LeCun and Geoffrey Hinton. Deep learning. *Nature*, 521(7553):436–444, 2015.

[70] Jimmy Ba Diederik Kingma. Adam: A method for stochastic optimization. *3rd International Conference for Learning Representations, San Diego*, 2015.

[71] Chollet Francois et. al. Keras. *published by GitHub*, 2015.

[72] N. Boulanger-Lewandowski Y. Bengio and R. Pascanu. Advances in optimizing recurrent networks. *In Proc. ICASSP 38*, 2013.

[73] T. Mikolov R. Pascanu and Y. Bengio. On the difficulty of training recurrent neural networks. *In Proceedings of the 30th International Conference on Machine Learning (ICML13). ACM*, 2013.

[74] KyungHyun Cho Yoshua Bengio Junyoung Chung, Caglar Gulcehre. Empirical evaluation of gated recurrent neural networks on sequence modeling. *NIPS 2014 Deep Learning and Representation Learning Workshop*, 2014.

[75] S. Hochreiter. Untersuchungen zu dynamischen neuronalen netzen. diploma thesis, institut fur informatik, lehrstuhl prof. brauer, technische universitat munchen. *URL http:// www7.informatik.tu-muenchen.de/Ehochreit*, 1991.

[76] Association for the Advancement of Medical Instrumentation. Non-invasive sphygmomanometers - part 2: Clinical investigation of automated measurement type. 2013. *Arlington, VA. 2013. Available at www.aami.org.*

[77] Gary Marcus. Deep learning: A critical appraisal. *arXiv:1801.00631 [cs.AI].*